Measurement of ambient NO_3 reactivity: Design, characterization and first deployment of a new instrument

Jonathan M. Liebmann[1], Gerhard Schuster[1], Jan B. Schuladen[1], Nicolas Sobanski[1], Jos Lelieveld[1] and John N. Crowley[1]

[1]Atmospheric Chemistry Department, Max-Planck-Institut für Chemie, 55128 Mainz, Germany.

Correspondence to: John N. Crowley (john.crowley@mpic.de)

Abstract. We describe the first instrument for measurement of the rate constant (s^{-1}) for reactive loss (i.e. the total reactivity) of NO_3 in ambient air. Cavity-ring-down spectroscopy is used to monitor the mixing ratio of synthetically generated NO_3 (≈ 30-50 pptv) after passing through a flow-tube reactor with variable residence time (generally 10.5 s). The change in concentration of NO_3 upon modulation of the bath gas between zero-air and ambient air is used to derive its loss rate constant, which is then corrected for formation and decomposition of N_2O_5 via numerical simulation. The instrument is calibrated and characterized using known amounts of NO and NO_2 and tested in the laboratory with an isoprene standard. The lowest reactivity that can be detected (defined by the stability of the NO_3 source, instrumental parameters and NO_2 mixing ratios) is 0.005 s^{-1}. An automated dilution procedure enables measurement of NO_3 reactivities up to 45 s^{-1}, this upper limit being defined mainly by the dilution accuracy. The typical total uncertainty associated with the reactivity measurement at the centre of its dynamic range is 16 %, though this is dependent on ambient NO_2 levels. Results from the first successful deployment of the instrument at a forested mountain site with urban influence are shown and future developments outlined.

1 Introduction

Large amounts of biogenic and anthropogenic trace gases are emitted annually into the atmosphere. Recent estimates (Guenther et al., 2012) suggest that about 1000 Tg of biogenic volatile organic compounds (bVOC), especially isoprene (contributing 50 %) and monoterpenes (15 %) are emitted annually by vegetation. The global burden of anthropogenic emission is dominated by CO_2, CO, N_2O, CH_4, SO_2, NO_2 and organic carbon, the latter contributing about 11 Tg (Huang et al., 2015). In particular, nitrogen oxides from combustion and microbial activity in soils have a major impact on the chemistry of the natural atmosphere (Crutzen, 1973). Most VOCs are oxidized efficiently in the Earth's boundary layer, the oxidizing capacity of which represents 15% of that of the entire atmosphere (Lelieveld et al., 2016). Biogenic and anthropogenic VOCs have a significant impact on air quality and human health and knowing and understanding their lifetimes, which are determined by the oxidizing capacity of the atmosphere, is prerequisite to predicting future atmospheric composition and related climate phenomena (Lelieveld et al., 2008).

During daytime, photochemically formed OH radicals represent the dominant contribution to the oxidative capacity of the atmosphere. As OH levels are vastly reduced in the absence of sunlight, the NO_3 radical (formed by reaction of NO_2 with O_3, R1) is the major oxidizing agent at elevated NO_x for many biogenic terpenoids and other unsaturated compounds at night-time (Wayne et al., 1991; Atkinson, 2000; Atkinson and Arey, 2003a, b; Brown and Stutz, 2012; Ng et al., 2016).

$$NO_2 + O_3 \rightarrow NO_3 + O_2 \quad \text{(R1)}$$

NO_3 reacts rapidly with NO (R2, rate constant 2.6×10^{-11} cm^3 $molecule^{-1}$ s^{-2} at 298 K (Atkinson et al., 2004)) and undergoes rapid photolysis (R5, R6) so that its lifetime is usually of the order of seconds during the day and its concentration too low for it to be considered an important daytime oxidant.

At night, NO_3 can react with NO_2 forming N_2O_5, which thermally decomposes to set up a thermal equilibrium between NO_2, NO_3 and N_2O_5 (R3, R4) with N_2O_5 formation favoured by lower temperatures. As both NO_3 and N_2O_5 are formed from NO_x ($NO_x = NO + NO_2$) the loss of either NO_3 via gas-phase losses or N_2O_5 via heterogeneous uptake to particles or deposition implies a reduction in NO_x, and thus a reduction in the rate of photochemical O_3 formation (Dentener and Crutzen, 1993). In addition, heterogeneous loss of N_2O_5 can also result in release of $ClNO_2$ from chloride containing particles (R7) (Osthoff et al., 2008; Thornton et al., 2010; Mielke et al., 2011; Phillips et al., 2012; Riedel et al., 2012). The main loss processes of NO_3 are summarised in Fig. 1.

$$NO_3 + NO \rightarrow 2\ NO_2 \quad \text{(R2)}$$

$$NO_2 + NO_3 + M \rightarrow N_2O_5 + M \quad \text{(R3)}$$

$$N_2O_5 + M \rightarrow NO_3 + NO_2 + M \quad \text{(R4)}$$

$$NO_3 + h\nu \rightarrow NO_2 + O \quad \text{(R5)}$$

$$NO_3 + h\nu \rightarrow NO + O_2 \quad \text{(R6)}$$

$$N_2O_5 + \text{surface} \rightarrow NO_3^- \text{ (and/or } ClNO_2) \quad \text{(R7)}$$

In rural and forested areas reaction with biogenic VOCs can dominate the loss of NO_3 (Mogensen et al., 2015). Especially terpenoids like limonene (k = 1.2 x 10^{-11} cm^3 $molecule^{-1}$ s^{-1}), α-pinene (k = 6.2 x 10^{-12} cm^3 $molecule^{-1}$ s^{-1}) and isoprene (k = 6.5 x 10^{-13} cm^3 $molecule^{-1}$ s^{-1}) have high rate constants for reaction with NO_3 (IUPAC, 2016; Ng et al., 2016). Under such conditions, when NO_x levels are low, NO_3 mixing ratios may be sub-pptv and below the detection limit for most instruments (Rinne et al., 2012).

The reaction of NO_3 with traces gases containing unsaturated C=C bonds proceeds via addition to form nitroxy-alkyl radicals that undergo rapid reaction with O_2 to form nitroxy-alkyl peroxy radicals. The peroxy radicals react further (with HO_2, NO, NO_2 or NO_3,) to form multi-functional organic nitrates, which can contribute to generation and growth of secondary organic aerosols (Fry et al., 2014; Ng et al., 2016) or be lost by deposition.

The role of NO_3 as an oxidizing agent may be assessed via its total reactivity (or inverse lifetime). Whereas for OH, experimental methods for measuring total reactivity in ambient air exist (Kovacs and Brune, 2001; Sinha et al., 2008), NO_3 reactivity has not yet been directly measured. Stationary-state approximations have often been used to calculate NO_3 lifetimes from its mixing ratio and production rate, the latter being given by: $k_1[NO_2][O_3]$ (Heintz et al., 1996; Geyer and Platt, 2002; Brown et al., 2007a; Brown et al., 2007b; Brown et al., 2009; Sobanski et al., 2016b). Thus the stationary-state turnover lifetime, τ_{ss}, can be calculated according to expression 1.

$$k_{ss} = \frac{1}{\tau_{ss}} = \frac{k_1\,[O_3]\,[NO_2]}{[NO_3]} \quad (1)$$

This method is applicable when the chemical lifetime of NO_3 is sufficiently short so that stationary-state can be achieved within transport time from emission to measurement location (Brown et al., 2003). Formally it is achieved when the production and loss of NO_3 and N_2O_5 are balanced (Brown et al., 2003; Crowley et al., 2011). The time to acquire stationary-state depends on production and loss rates for NO_3 and N_2O_5 and can take several hours. This approach can break down under conditions of moderate to high NO_2 levels, strong sinks, low temperatures, or very clean air masses in which the sinks for NO_3 and N_2O_5 become small (Brown et al., 2003). Indeed, Sobanski et al. (2016b) observed much lower stationary-state loss rates compared to those calculated from measured VOC mixing ratios during the PARADE 2011 campaign and concluded that this was mainly the result of sampling from a low lying residual layer with VOC emissions that were too close for NO_3 concentrations to achieve stationary-state. They also considered the possibility that NO_3 may be formed by the oxidation of NO_2 by Criegee Intermediates, which would bias calculations of its reactivity.

Summarizing, NO_3 reactivity with respect to gas-phase losses is a direct indication of night-time oxidation rates of VOCs, with direct impacts on NO_x levels by forming long-lived reservoir species (alkyl nitrates) some of which will partition to the particle phase. Via modification of N_2O_5 concentrations (formed in an association reaction of NO_3 with NO_2, R3), the NO_3 reactivity indirectly controls heterogeneous NO_x losses and $ClNO_2$ formation rates.

In this paper we describe a newly developed instrument that enables point measurements of NO_3 reactivity in ambient air. After introducing the methodology in section 2, we show the results of extensive laboratory characterization of the

instrument along with discussion of the uncertainties associated with those measurements in section 3 to 5. In section 6 we present a dataset of ambient NO_3 reactivity obtained at a forested / urban location in south-western Germany.

2 Methodology

Our experiments to measure NO_3 reactivity involve comparison of loss rates of synthetically generated NO_3 in zero-air and in ambient air introduced into a flow-tube reactor. In zero-air, the loss of NO_3 is due to its reaction with NO_2 (present as a necessary component in the generation of NO_3, see below) and losses on surfaces of the flow-tube. When zero-air is replaced by ambient air, NO_3 is additionally removed by reaction with reactive gases present and its mixing ratio reduced accordingly. An analysis of the change in signal for a fixed reaction time enables the NO_3 reactivity to be derived once certain corrections have been applied (see below).

Figure 2 displays a schematic diagram of the experimental set-up. The three central components are a dark reactor for generation of NO_3, the flow-tube in which NO_3 reacts with trace gases in ambient air samples and the detection system for NO_3.

2.1 Generation of NO_3

Many laboratory studies of NO_3 kinetics have used the thermal decomposition of N_2O_5 as NO_3 source (R4) (Wayne et al., 1991). The generation of NO_3 from gas-phase N_2O_5 eluted from samples of crystalline N_2O_5 (at -80 °C) was found to be insufficiently stable for the present application and is also difficult (though not impossible, see e.g. (Fuchs et al., 2008; Wagner et al., 2011)) to use during field campaigns where adequate laboratory facilities for the safe generation and purification of N_2O_5 are frequently not available. In addition, generation of NO_3 from N_2O_5 was also accompanied by an NO_2 impurity of several parts per billion (ppbv).

We therefore generate NO_3 and N_2O_5 in situ, via the oxidation of NO_2 by O_3 (R1, R3). For this purpose, 400 standard cm^3 min^{-1} (sccm) of synthetic air from a zero-air generator (Fuhr Cap 180) are passed over a Hg lamp (low-pressure, Penray type) at a pressure of 1200 Torr. The photo-dissociation of O_2 at 184.95 nm results in formation of oxygen atoms that recombine with O_2 to form ≈ 400 ppbv O_3. The O_3 / air flow is then mixed with NO_2 in synthetic air (0.93 ppmv, 1-10 sccm) and directed into a temperature stabilized (30 °C), darkened, FEP coated reactor (length 70 cm, diameter 6 cm) also at a pressure of 1200 Torr. The reactor is darkened to prevent the photolysis of NO_3 by room lights. Operation at above-ambient pressure extends the reaction time for a given flow rate, thus optimising the conversion of NO_2 to NO_3 via the reaction between NO_2 and O_3, which has a low rate constant of 4.05×10^{-17} cm^3 $molecule^{-1}$ s^{-1} at 30 °C. The use of high pressures also optimises the formation of N_2O_5 in the termolecular reaction R3, and reduces the rate of diffusion and loss of NO_3 to the walls of the reactor. A high pressure in the darkened reactor also has the advantage of decoupling it from fluctuations in ambient pressure which influence the formation of N_2O_5. Heating the reactor to above room-temperature is carried out to stabilise the formation of N_2O_5, which otherwise shows strong fluctuations owing to variations in laboratory temperature, typically about

3-5 degrees within the course of a day or night. The approximate reaction time for the stepwise conversion of NO_2 to N_2O_5 in the darkened reactor is ≈ 5 min. Based on the O_3 concentration and the rate constant for R1, the initial conversion of NO_2 to NO_3 is about 15%.

The gas exiting the darkened reactor passes through a pin-hole (Ø ≈ 250 µm) to reduce the pressure to roughly ambient level and then enters a ≈ 30 cm long piece of ¼ inch (≈ 6.4 mm) PFA tubing (residence time ≈ 0.5 s) which is heated to 140 °C in order to thermally decompose N_2O_5 to NO_3. Calculations using the thermal decomposition rate constant for N_2O_5 (lifetime = 0.001 s at 140°C) indicate that after ≈ 0.1 s the N_2O_5 is stoichiometrically converted to NO_3. The temperature is measured on the outside of the PFA tubing and does not necessarily reflect the temperature of the gas flowing through it. The value of 140 °C is chosen based on a series of experiments in which the tubing temperature was varied and the yield of NO_3 monitored. A PFA T-piece located immediately behind the heated tubing is used to add a 2900 sccm flow of either zero- or ambient-air to the synthetic NO_3 sample. After this dilution step the air contains ≈ 50 pptv NO_3, ≈ 1 ppbv NO_2 and ≈ 50 ppbv O_3. As described later, keeping NO_2 and O_3 levels as low as possible has important consequences for the data analysis. Low levels of NO_3 also help to ensure that the addition of NO_3 does not significantly change the reactivity of the air, i.e. by removing a large fraction of the reactive trace gases. We later assess the potential change in air-mass reactivity (i.e. by depletion of reactive trace gases of formation of reactive radicals) following addition of NO_3 at these levels to ambient air.

As described below, the present instrument is a modification of one designed to measure ambient mixing ratios of NO_3 and N_2O_5 and is equipped with a second cavity connected to a heated inlet that measures the sum of NO_3 and N_2O_5. Experiments in which both cavities were used to analyze the flow out of the heated piping indicated that there was no residual N_2O_5.

2.2 Detection of NO_3 using cavity-ring-down spectroscopy

For detection of the NO_3 radical we used Cavity Ring-Down Spectroscopy (CRDS), a sensitive technique for measurements of atmospheric trace gases and often used for measurement of ambient NO_3 (Brown et al., 2002). In essence, CRDS is an extinction measurement in a closed optical resonator (cavity) where light is trapped between mirrors with high reflectivity to generate a very long absorption path. Ring-down refers to the decay of light intensity (monitored behind the cavity exit mirror) and the general expression to derive the concentration of an absorbing or scattering gas is given by (Berden et al., 2000):

$$[X] = \frac{1}{c\sigma_{(x,\lambda)}}\left(\frac{1}{\tau_X} - \frac{1}{\tau_0}\right) \quad (2)$$

Where τ_0 and τ_x correspond to decay constants in the absence and presence of an absorbing or scattering trace gas X, respectively and $\sigma_{(X,\lambda)}$ is the absorption cross-section / scattering coefficient of X at wavelength λ.

The instrument used is a two-channel CRDS that was previously used to measure ambient levels of N_2O_5 and NO_3 (Schuster et al., 2009; Crowley et al., 2010). Important modifications to the previous set-up include use of FEP coated glass cavities of equivalent size and fibre-optics for the coupling of the laser to the cavity. The thermal dissociation cavity previously used for detection of atmospheric N_2O_5 is not necessary for the measurement of NO_3 lifetimes but was used for calibration and

characterization experiments. Only the central features and important modifications compared to the prototype described in Schuster et al., (2009) are described in detail here.

The light source is a 625 Hz, square-wave modulated, 100 mW laser-diode located in a Thor Labs TCLDM9 housing and thermally stabilized at 36°C using a Thor Labs ITC 502 Laser-Diode Combi Controller to produce light at 661.95 nm (0.5 nm full width at half maximum) and therefore close to the NO_3 absorption maximum. The effective cross section of NO_3 was calculated as 2.09 x 10^{-17} cm^2 $molecule^{-1}$ by convoluting the temperature dependent NO_3 absorption spectrum (Orphal et al., 2003; Osthoff et al., 2007) with the laser-diode emission spectrum. Coupling between the laser-diode and the cavities is achieved by using either optical fibres (0.22 NA, 50 µm core, 400-2400 nm) for measuring NO_3 reactivity or using fibre-optics with a beam splitter (Thor Labs FCMM50-50A-FC, 50:50 ratio) in order to operate both cavities. The beam was collimated (Thor Labs FiberPort Collimator PAF-X-18-PC-A) and directed through an optical isolator (Thorlabs IO-3D-660-VLP), focused by a lens (Thorlabs A230TM-A) into the optical-fibre and then collimated again to a beam diameter of about 6 mm before entering the cavity.

The NO_3 cavity (Teflon-coated glass (DuPont, FEP, TE 9568), length 70 cm, volume 79cm^3) was operated at room temperature, while the N_2O_5 cavity was operated at 80°C with a pre-cavity section heated to 85°C in order to convert N_2O_5 to NO_3. The NO_3-cavity was connected to the flow-tube using 1/8" (≈ 3.2 mm) PFA tubing that lined the 1/4" (≈ 6.4 mm) injector. The use of small diameter tubing results in short transport times between the flow-tube and CRDS and also induces a pressure drop of 133 mbar, so that the pressure in the cavity was 880 mbar. Gases entered the middle of the cavity via a T-piece and were pumped from the ends via a flow controller into the exhaust. The flow rates in both cavities were 3000 cm^3 (STP) min^{-1} (sccm) resulting in a residence time of approximately 1.6 s as calculated from the volume flow. Gas entering the CRDS detector was always passed through a 2 µm membrane filter (Pall Teflo) to remove particles. Light exiting the cavities through the rear mirror was detected by a photomultiplier (Hamamatsu E717-500) which was screened by a 662 nm interference filter. The pre-amplified PMT signal was digitized and averaged with a 10 MHz, 12 bit USB scope (Picoscope 3424) which was triggered at the laser modulation frequency of 625 Hz.

The ring-down constant in the absence of NO_3 was obtained by adding NO (1-3 sccm of a 100 ppmv mixture NO in N_2) every 40 points of measurement for approximately 15 s. Titration with NO took place at the inlet of the T-shaped glass cavity giving the gas mixture sufficient time to react with NO_3. The *L/d* ratio (the ratio of the distance between the cavity mirrors (*L*) and the length of the cavity that is filled by absorber (*d*)) was determined as described previously (Schuster et al., 2009; Crowley et al., 2010) and was 1.01 ±0.03. Values of τ_0 in dry zero-air at 760 Torr were usually between 140 and 160 µs indicating optical path lengths of ≈ 42-48 km. When operated at a flow of 3000 sccm, the noise levels on the NO_3 signal are such that the precision (3s integration interval) is better than 1 pptv. As we describe later, the NO_3 reactivity is derived from measurements of the relative change in the NO_3 mixing ratio, so that the precision rather than total uncertainty in the NO_3 mixing ratio defines the accuracy of the reactivity measurement.

2.3 Flow-tube for NO_3 reactivity measurement

The flow-tube, thermostatted to 20 °C by flowing water through an outer jacket, is an FEP-coated glass tube of length 50 cm and internal diameter 4 cm. Gas enters the flow-tube at one end via a conical section with a 3/8 inch (≈ 9.5 mm) glass fitting through which ¼ inch (≈ 6.4 mm) PFA tubing could be inserted. The total flow through the flow-tube was 3300 sccm, consisting of 400 sccm from the darkened reactor and 2900 sccm zero-air / ambient air. The flow and pressures indicated above, result in a Reynolds number of ≈ 123 (i.e. laminar flow) in the cylindrical part of the flow-tube, but with an entrance length (Le) to acquire laminar flow of 27 cm indicating that the flow-tube operates in a mixed turbulent / laminar flow regime.

$$Le = 0.112\, r\, Re \quad (3)$$

Gases exit the flow-tube via a length of 1/8 inch PFA tubing supported in an axially centred stainless-steel tube (length 50 cm, diameter ¼ inch) which could be translated along the major flow-tube axis thus changing the contact (reaction) time between NO_3 and any reactive species or the flow-tube wall. In principal, this enables the dynamic range of the measurement to be adjusted (i.e. long contact times for low reactivity, short contact times for high reactivity) though we found that reactivity-dependent dilution of the ambient air was a better method to extend the dynamic range to high reactivities as very short reaction times were not possible due to a finite residence time in the CRDS detection system and also due to mixing effects in the flow-tube. In order to prevent formation of a "dead volume" at the back of the flow-tube beyond the tip of the outlet, 400 sccm were removed via a critical orifice to the exhaust pump. During measurement of NO_3 reactivity the extraction point was usually set for a reaction time of about 10.5 s, which was determined as described below.

As described later, to derive the NO_3 reactivity we compare its concentration in zero-air to that in ambient air samples. We found that when switching between sampling ambient air and dry, zero-air, the resulting change in relative humidity caused an abrupt change in NO_3 which then slowly recovered towards its original value. Measurement of the wall loss rate of NO_3 in dry and humidified zero-air by moving the injector (see below) revealed no substantial difference and we conclude that the change in NO_3 is due to wall loss at the point of mixing of NO_3 flows and the zero-air flow, which is very turbulent. In order to eliminate data loss while waiting for signals to stabilise following zeroing, we humidify the zero-air to the same absolute humidity (±2 %) as ambient. To do this, the ambient relative humidity was monitored by passing 100 sccm air over a sensor that recorded both temperature and relative humidity. The zero-air was humidified by directing a variable fraction of the (constant) total flow through a 2 l gas wash-bottle filled with HPLC grade water. The relative humidity of the resulting mixture was matched to ambient levels by dynamic adjustment of the fractional flow passing through the wash-bottle. The zero-air used for purging the mirrors as well that used for NO_3 generation was not humidified.

In order to ensure that air from the zero-air generator was free of reactive gases that survived the catalytic purification process, we compared it to hydrocarbon-free, bottled synthetic air (Westfalen). No change in the concentration of [NO_3] could be observed when switching between zero-air and bottled air, indicating that the zero-air generator was suitable.

However, poisoning of the catalyst of the zero-air generator by amines, sulphides or thiols or contamination of the filters could potentially become problematic when using compressed, highly polluted ambient air.

2.3.1 Derivation of the effective reaction time and wall loss rate constant for NO_3

In flow-tubes where radial, diffusive mixing of gases is rapid (i.e. at low pressures of He and "plug-flow" conditions), the effective reaction time can be close to that calculated from the volumetric flow rate once axial diffusion is accounted for (Howard, 1979). At higher pressures and laminar flow, reactions times are defined by the parabolic velocity distribution and extent of radial mixing whereas high pressure flow-tubes operated under turbulent conditions (Reynold numbers > 3000) plug-flow can be achieved (Seeley et al., 1993; Donahue et al., 1996). According to the calculations of Reynolds numbers outlined above, our flow-tube is not operated in either a pure laminar or turbulent regime, which can make accurate calculation of the reaction time difficult. Using the volumetric flow rate and flow-tube diameter, we calculate an average, linear velocity of the gas of 4.78 cm s^{-1} at 760 Torr and 298 K in the cylindrical section of the flow-tube. This enables us to calculate the injector position dependent reaction time in the flow-tube, which for 45 cm is 9.5 s. This should be regarded as an initial estimate of the true reaction time as it does not consider the non cylindrical section of the flow-tube (2.5 % of total volume), the radial distribution of velocities in the flow-tube or mixing effects. A further additional 1.6 s must be added to this to take the average reaction time in the cavity into account (calculated from the cavity volume and the flowrate) resulting in an approximate, total reaction time of 11.1 s.

A further method to derive an "effective" or averaged reaction time is to add a short pulse of gas to the flow-tube and monitor its arrival time at the detector. However, as NO_3 cannot be easily stored, we instead add a pulse of a reactant that removes NO_3. A syringe was therefore used to add a short pulse (0.1 cm^3 in < 0.5 s) of NO diluted in N_2 (0.22 ppbv) to the flow-tube at the T-piece where the NO_3 source and zero-air are mixed.

The resultant depletion in the NO_3 signal (measured at a time resolution of 0.35 s) displayed an inverted Gaussian form with an elongated flank after the minimum (Fig. 3) which can be attributed to non-isothermal effects, secondary flows and recirculation processes in the flow-tube (Huang et al., 2016) which require fluid dynamics simulations to be fully characterised. The average reaction time, *t*, can however be derived from:

$$t = \frac{\sum I_j t_j}{\sum I_j} \quad (4)$$

where I_j is the signal recorded at each time step t_j

In total, 25 experiments were conducted, resulting in an effective reaction time of 11.4 ± 0.5 s determined via expression (4). The two methods outlined above thus provide approximate values for the reaction time which are in good agreement (< 3 % deviation).

As the reaction time is a central parameter for calculating the NO_3 reactivity, a third method was employed, in which a known amount of NO was added at the usual mixing point and the depletion in NO_3 observed. As the rate constant for reaction of NO with NO_3 is known with an uncertainty (at room temperature) of 13 %, this should enable derivation of an

effective reaction time that also takes all mixing effects (both in the flow-tube and cavity) into account. In a series of experiments, known amounts NO were added to the 2900 sccm flow of zero-air (via a calibrated mass flow controller) at the usual mixing point. In the absence of other processes which remove or form NO_3, its change in concentration upon adding NO is described by:

$$[NO_3]_t = [NO_3]_0 \, exp^{-(k_2[NO]+k_w+k_3[NO_2])t} \quad (5)$$

Where $[NO_3]_0$ and $[NO_3]_t$ are the concentrations of NO_3 before and after addition of NO, respectively. k_2 and k_3 are the rate constants for reaction of NO_3 with NO and NO_2, respectively at the flow-tube / cavity temperature, k_w is the rate constant (s^{-1}) for loss of NO_3 at the flow-tube walls and t is the desired parameter. Rearranging, we get a simple expression (6), which shows that a plot of $\ln([NO_3]_t)$ versus [NO] should yield a slope of k_2t, from which t can be derived using an evaluated and recommended value of k_2 (Atkinson et al., 2004). Once corrected for the contribution from $k_5[NO_2]$, the intercept should, in principal, give a value of k_w.

$$ln\frac{[NO_3]_0}{[NO_3]_t} = k_2[NO]t + k_w + k_3[NO_2] \quad (6)$$

A plot of $[NO_3]_t$ versus [NO] is displayed in Fig. 4a for three different amounts of added NO_2. Although the curve follows roughly exponential behaviour as expected, the slopes and thus the value of t obtained was found to depend on the initial NO_2 concentration, with values of 5.7, 5.1 and 4.5 s obtained for NO_2 mixing ratios of 2.94, 5.88 and 8.82 ppbv, respectively. This indicates that the kinetics of NO_3 formation and loss are more complex than defined by expression (6) and the relative rates of reaction of NO_3 with NO (R2) and NO_2 (R3) and its formation via N_2O_5 decomposition (R4) and reaction of O_3 with NO_2 (R1) in the flow-tube all impact on the NO_3 mixing ratio. In Fig. 4b we display the results of a similar experiment in which NO_2 as added. In this case, there is obvious curvature in the plot of $[NO_3]_t$ versus $[NO_2]$, which is not predicted by expression (5). The decomposition of N_2O_5 formed by reaction R3 as well as oxidation of NO_2 by O_3 (R1, see section 3.1) both lead to the formation of NO_3 and are the causes of this behaviour, especially at high $[NO_2]$ and low [NO]. At the flow-tube and cavity temperature (circa 298 K), the rate constant for decomposition of N_2O_5 (k_4) is 4.4×10^{-2} s^{-1} (Atkinson et al., 2004).

Extraction of the reaction time thus required numerical simulation of the data obtained by adding various amounts of NO, to the flow-tube in the presence of different NO_3 and NO_2 concentrations. The impact of reactions R2, R3 and R4 was assessed by numerical simulations using FACSIMILE (Curtis and Sweetenham, 1987) and considering the reactions listed in Table 1. The input parameters for the simulations were the concentrations of NO, NO_2 and O_3 and the rate constants, which were taken from IUPAC recommendations (Atkinson et al., 2004). The total reaction time (t) and the wall-loss rate constant for NO_3 (k_w) were adjusted until each of the six datasets could be reproduced with a single value for each parameter. The initial concentration of $[NO_3]_0$, was allowed to float until best agreement was achieved. This way, the reaction time was determined to be 10.5 s, which is in good agreement with that derived by pulsed addition of NO. As our reactivity derivation relies on the change in NO_3 signal upon adding a reactant to the flow-tube, we consider the value of 10.5 s, which takes mixing,

diffusion etc. into account to be the most appropriate value but assign an uncertainty (± 1 s) that overlaps with the other methods. The wall loss rate of NO_3 (which is independent of the NO and NO_2 concentrations) was found to be 4×10^{-3} s^{-1}.

For analysis of ambient reactivity we use a reaction time of 10.5 s as derived from the addition of NO. This means that our ambient reactivities are directly tied to the rate constant for reaction between NO_3 and NO. As described later, during ambient measurements we periodically add a known amount of NO to the zero-air to monitor a known reactivity under real operating conditions.

Figures 5a and 5b show the correlation between simulated and measured NO_3 concentrations in these experiments. In both cases the slope is close to unity (0.97-1.02) with an intercept close to zero. A set of similar experiments performed at 30 % and 80 % humidity also showed excellent agreement using the same values of t and k_w. We conclude that the behaviour of NO_3 in this system can be very accurately predicted by numerical simulations using a simple reaction scheme under a variety of conditions (initial NO_3, NO and NO_2 varied), giving us confidence in our ability to extract loss rates for NO_3 in ambient air.

When gas-phase reactivity is low, a substantial fraction of NO_3 may be lost via collisions with the walls rather than due to reactive gases. For this reason, we re-measured the value of k_w obtained above in a further set of experiments in which the NO_3 concentration was measured as a function of injector position (contact time in the flow-tube) at a constant initial mixing ratio of NO_3 and NO_2 and in the absence of NO. For this we calculate the reaction time for each of the three injector positions from pulsed addition of NO as described above, but normalized to the reaction time derived from addition of NO with numerical simulation. The results of such an experiment are displayed in Fig. 6 and we draw attention to the fact that, even at maximum reaction time (10.5 s), the change in the NO_3 concentration is only about 10 %. This reflects the low efficiency of reaction of NO_3 with the FEP coated glass walls. Similar experiments performed before and after the NOTOMO campaign (see below) indicated that the FEP coating did not degrade significantly following sampling of filtered, ambient air. The numerical simulation was initialised with the same set of rate parameters described above, a fixed NO_2 concentration and only k_w and the initial NO_3 concentration were varied. The best fit was obtained when k_w was 4×10^{-3} s^{-1}, in agreement with the simulations at fixed time and variable NO and NO_2. Using expression (7) where r is the flow-tube radius, $\bar{c}$ the mean molecular speed and which assumes laminar flow and no diffusive limitation to uptake, this value of k_w can be converted to an approximate uptake coefficient for NO_3 to the FEP-coated tube of $\approx 5 \times 10^{-7}$.

$$\gamma = \frac{2\,r\,k_w}{\bar{c}} \qquad (7)$$

3 Data analysis and derivation of NO_3 reactivity

We first consider the passage of NO_3 through the flow-tube in a flow of zero-air. If NO_3 is lost in one or more pseudo-first-order processes, its decay should be exponential and its concentration, $[NO_3]_t^{ZA}$ after a reaction time t, is given by expression (8).

$$[NO_3]_t^{ZA} = [NO_3]_0^{ZA} exp^{(-k_{ZA}t)} \quad (8)$$

Where the superscript "ZA" refers to use of zero-air. As NO_3 is lost only via reaction with NO_2 and to the wall, $k_{ZA} = k_{wall} + k_{NO2}$ where k_w is the first-order loss rate constant for wall-loss and k_{NO2} is the first-order loss rate constant for reaction with NO_2 and is equal to $k_3[NO_2]$. When zero-air is switched for ambient air containing reactive trace gases (RTG), we have:

$$[NO_3]_t^{Amb} = [NO_3]_0^{Amb} exp^{(-k_{Amb}t)} \quad (9)$$

where $k_{Amb} = k_w + k_{NO2} + k_{RTG}$ and k_{RTG} is the first-order loss rate constant for reaction of NO_3 with trace gases present in ambient air other than NO_2.

If $[NO_3]_0^{ZA}$ and $[NO_3]_0^{Amb}$ are equivalent, expression 10 is obtained.

$$\frac{[NO_3]_t^{ZA}}{exp^{(-k_{ZA}t)}} = \frac{[NO_3]_t^{Amb}}{exp^{(-k_{Amb}t)}} \quad (10)$$

Rearranging and substituting for k_{ZA} and k_{Amb} leads to

$$k_{RTG} = \frac{\ln\left(\frac{[NO_3]_t^{ZA}}{[NO_3]_t^{Amb}}\right)}{t} = 1/\tau \quad (11)$$

Where τ is the NO_3 lifetime. In principal, it should thus be possible to calculate the reactivity of NO_3 in ambient air by measuring $[NO_3]_t^{ZA}$, $[NO_3]_t^{Amb}$ and knowing the reaction time *t.* Later we discuss the applicability of this expression and show that corrections are necessary to take the re-formation of NO_3 into account, especially when dealing with air-masses with high NO_2 content. This is similar to the laboratory experiments described above and required numerical simulation, which we present below.

The concentration of NO_3 in zero-air measured when the injector is positioned for maximum reaction time, $[NO_3]_t^{ZA}$, was measured by flushing the inlet with 3000 sccm zero-air creating an overflow of ≈ 100 sccm. When switching to ambient measurements, the zero-air overflow was redirected via a flow controller, F_3, that connected the zero-air overflow line to the exhaust and which was set to 3500 sccm. This setup has the advantage of enabling dynamic dilution of ambient air. If the reactivity is so high that the NO_3 levels approached the detection limit, F_3 does not withdraw the entire 3500 sccm overflow but allows e.g. 2000 sccm to be added to the inlet, resulting in sampling 900 sccm of ambient air plus 2000 sccm of zero-air, a dilution factor of 2900/900 which is slightly increased by the 400 sccm flow from the darkened reactor. A five point dynamic dilution with zero-air is implemented in the software, which changes the set point for F_3 and dilutes the ambient air with zero-air if $[NO_3]_t^{Amb}$ decreases below 10 pptv for an average time period of 30 s. Conversely, the dilution can be decreased again if $[NO_3]_t^{Amb}$ becomes $\geq [NO_3]_t^{ZA} - 10$ ppt. Dilution factors (D_i) were determined using a Gilibrator flow meter (Gilian Gilibrator-2) and were: D_1=1.14 for the measurement of pure ambient air (here the small dilution effect is caused by the 400 sccm zero-air used in the production of NO_3), D_2=1.74, D_3=3.71, D_4=8.98, D_5=14.07 when diluting ambient air. With increasing dilution, errors in the measurement will increase as well (see later).

The analytical expression given above to derive the NO_3 reactivity is an ideal case in which NO_3 is lost by a number of first-order processes and is not formed in the flow-tube to a significant extent. However, as we already demonstrated in the

laboratory experiments to examine the effects of varying NO, NO_2 and NO_3 concentrations, the formation of N_2O_5 in the reaction of NO_3 with NO_2 (R3) and its thermal decomposition back to NO_3 can impact on the NO_3 concentration as NO_2 is present both in the mixture used to generate N_2O_5 and NO_3 and also in ambient air. While the formation of N_2O_5 from NO_2 and NO_3 (R2) is, to a good approximation, independent of temperature between about 280 and 305 K, the rate constant for thermal decomposition of N_2O_5 (R3) varies by a factor of 26 over the same temperature range. The simple, analytical approach outlined above thus fails at temperatures where the decomposition of N_2O_5 is important and when sufficient NO_2 is present to account for a significant fraction of the loss of NO_3. This is illustrated in Fig. 7a, in which simulations of the NO_3 concentration at a reaction time of 10.5 s and at different temperatures and amounts of NO_2 (as reactant) are displayed and compared with the simple exponential behaviour (black data points) calculated from expression (11). The simulations show that the dependence of the NO_3 concentration on NO_2 is non-exponential, indicating that re-generation of NO_3 from the N_2O_5 formed is significant, especially at higher temperatures. Figure 7b plots the ratio of the true reactivity (i.e. that used as input into the numerical simulation) versus that obtained by analyzing the simultaneous change in NO_3 concentration using expression (11). It is evident that the use of this expression generally results in underestimation of the true reactivity due to the formation and decomposition of N_2O_5. The bias will be largest when sampling polluted air where the reactivity has a large component due to NO_2 and small under conditions of low NO_2 and high k_{RTG} typical for remote, forested areas. However as previously mentioned the decomposition of N_2O_5 is strongly temperature dependent so that the bias will increase with rising temperature and decrease with sinking flow-tube temperature.

Apart from the formation and thermal dissociation of N_2O_5, the reaction of NO_2 with O_3 may, under some conditions, represent a further potential source of NO_3 in the flow-tube despite the low rate constant for (R1). Due to the in-situ method of production of N_2O_5 and NO_3 in the dark reactor, NO_2 (0.6-3 ppbv) and O_3 (40-50 ppbv) are always present in the flow-tube. NO_3 generated in the flow-tube was therefore simulated for different amounts of O_3 and NO_2 corresponding to the minimum and maximum mixing ratios used in our experiments. Figure 8 indicates that with 50 ppbv of O_3 and 2 ppbv NO_2, < 0.5 pptv of NO_3 is formed in the 10.5 s available for reaction in the flow-tube, which would not strongly impact on the results if the analytical expressions above were used to derive the NO_3 reactivity. Under highly polluted conditions (e.g. 100 ppbv O_3 and 20 ppbv NO_2) the effect is however measureable (> 2 pptv).

The discussion above indicates that the use of expression (11) can, under certain circumstances (e.g. low NO_x, high NO_3 reactivity to VOCs) give a reasonable representation of the NO_3 reactivity. However, in order to be able to derive NO_3 reactivities from any air mass we use numerical simulation take NO_3 reformation into account and enable extraction of accurate values in any conditions.

3.1 Numerical simulations for extraction of ambient reactivity

In this section we outline the experimental procedure and the associated data analysis for extracting the NO_3 reactivity from an ambient dataset as exemplified by the data shown in Fig. 9. This data covers a 1 hour period in which several phases of inlet-overfilling with humidified zero-air and titration with NO are apparent as are periods of mixing NO_3 with ambient air.

The dataset has already been corrected for baseline drift in the NO_3 zero during titration, hence each titration-zero is scattered around 0 pptv NO_3.

The periods marked "ZA" (zero-air) were used to extract the NO_3 concentration after a residence time of 10.5 s in flow-tube in the absence of ambient reactive trace gases. The data show that a plateau in the NO_3 signal with zero-air is observed after about 2-3 titration cycles are complete, which is the result of slow flushing through the inlet of reactive gases, which have extended surface residence times on the inlet material and fittings. Once a stable signal is acquired, $[NO_3]_{t=10.5}^{ZA}$ can be taken as an average value for each 300 s zero-air phase. These values are then used to calculate the initial NO_3 concentration $[NO_3]_0^{ZA}$, i.e. before NO_3 enters the flow-tube. This was done in an iterative procedure using numerical simulation with FACSIMILE embedded in a separate program. Input values are the O_3 and NO_2 concentration (from the darkened reactor), a first estimate for $[NO_3]_{t=0}^{ZA}$ and the rate coefficients for the NO_3 reactions listed in Table 1. At the end of the simulation (a few seconds of computing time) the simulated and measured values of $[NO_3]_{t=10.5}^{ZA}$ are compared and the ratio used to adjust the next input value for $[NO_3]_{t=0}^{ZA}$. The iteration continued until convergence was reached. Convergence was considered satisfactory when the deviation between measured and simulated values of $[NO_3]_{t=10.5}^{ZA}$ was less ≤1 %. This usually took only 5 simulations per data point as the initial value for each new time point was chosen to be the final value for the preceding time point. Ideally, $[NO_3]_{t=0}^{ZA}$ should be constant over long periods of time. In fact, deviations of several pptv, especially during field measurements, were observed over periods of hours and so values of $[NO_3]_{t=0}^{ZA}$ were linearly interpolated to each time point in which ambient reactivity was recorded.

Once initial NO_3 concentrations had thus been obtained a new set of simulations was started to simulate the measured values of $[NO_3]_{t=10.5}^{Amb}$. In this case, the simulation was initialized with the values of $[NO_3]_{t=0}^{ZA}$ obtained as described above and the total NO_2 concentration and O_3 concentrations, which contained a constant contribution from the dark-reactor and a variable concentration from ambient NO_2 and O_3 once corrected by the dilution factor (see above). An initial estimate of the total NO_3 reactivity, k_{RTG}, was made and the simulated value of $[NO_3]_{t=10.5}^{Amb}$ compared to that measured. The simulation was iterated, with incremental adjustment of k_{RTG} until agreement between simulation was ≤1 %. For ambient datasets, in which the reactivity can be highly variable this sometimes took several iterations, though as each simulation took less than a second this is not a particularly time consuming procedure.

4 Reactivity of an isoprene standard.

To validate our experimental and analytical procedure, we performed reactivity measurements on a bottled isoprene standard (0.933 ± 0.09 ppmv, Westfalen), diluted in zero-air. Isoprene was chosen as it is an important biogenic reactant for NO_3 in the troposphere and also because the rate coefficient, $k_{isoprene}$, for its reaction with NO_3 has been studied on many occasions (Atkinson et al., 2006; IUPAC, 2016) and therefore has a low associated uncertainty ($k_{isoprene}$ = 6.5 ± 0.15 x 10^{-13} cm^3 $molecule^{-1}$ s^{-1} at 298 K).

Experiments were carried out at various isoprene and NO_2 mixing ratios and the results are summarized in Fig. 10, which indicates excellent agreement between the measured reactivity and that calculated from the isoprene mixing ratio and rate coefficient, the slope of an unweighted fit being 1.00 ± 0.03. The error bars on the calculated reactivity represent total uncertainty in the isoprene and NO_2 mixing ratio, the reaction time and the rate coefficient. These results confirm that the instrument and data analysis procedure measure accurate values of NO_3 reactivity in the presence of NO_2 and organic reactants.

5 Detection Limit, dynamic range and overall uncertainty

While the overall uncertainty associated with absolute NO_3 concentration measurement are influenced by factors such as uncertainty in the cross-section as well as in the measurement of the laser emission spectrum the fractional change in concentration used to derive the NO_3 reactivity is not impacted. The detection limit for measuring NO_3 reactivity is defined by the minimal detectable change (MDC_{NO3}) in the NO_3 mixing ratio. This depends on noise levels and drift in ring-down-time, i.e. on the precision of the NO_3 signal and also on the stability of the synthetically generated NO_3. The instrumental noise on the NO_3 signal was reduced by averaging over ≈ 3 s per data-point (≈ 1800 ring-down-events) to give a noise limited detection limit (1 σ) of ~ 0.2 pptv. Precision is limited by the stability of the CRDS setup where changes in the mirror reflectivity induced by thermal or mechanical stress can lead to a drift in the ring-down time. The precision can be estimated from the standard deviation of the signal from one zeroing period to the next over the measurement period. Under typical laboratory conditions this was normally ≈ 0.7 pptv.

Since $[NO_3]_0^{ZA}$ is interpolated onto the measured $[NO_3]_t^{Amb}$ time series to calculate the reactivity, the stability of the NO_3 source is of great importance. Changes in the amount of synthetically generated NO_3 are caused by fluctuations in the temperature or pressure of the dark-reactor, the flow of NO_2 and changes in the intensity of light from the O_3 generator. In general, the poorer the stability of the NO_3 source chemistry, the more frequently the NO_3 mixing ratio in zero-air has to be measured. In laboratory conditions, changes of ±1 pptv within one hour were typical, making $[NO_3]_t^{ZA}$ measurements every 1200 s more than sufficient. In field conditions, where the instrument housing may be subject to larger temperature fluctuations, more frequent determination of $[NO_3]_t^{ZA}$ may be necessary. The NO_3 source stability was obtained from the standard deviation of the averaged $[NO_3]_t^{ZA}$ concentrations and propagating this with the standard deviation of two consecutive $[NO_3]_t^{ZA}$ measurements, for which typical values in laboratory conditions were ≈ 1 ppt. To define an overall, minimal detectable change in NO_3 (MDC_{NO3}), the noise and drift limited precision was combined with the NO_3 source stability to result in MDC_{NO3} = 2.5 pptv.

An MDC_{NO3} of 2.5 pptv results in a lower limit for the measurement of NO_3 reactivity of 0.005 s^{-1} (obtained from expression (11) with $[NO_3]_t^{ZA} = 50$ pptv and $[NO_3]_t^{Amb} = [NO_3]_t^{ZA} - MDC_{NO3} = 47.5$ pptv, at the lowest dilution factor of 1.14). An upper limit for the measurable reactivity is 45 s^{-1}, largely defined by the uncertainty of the dilution factor. Dilution factors

were obtained by measurements of the actual flows going into the flow-tube using a Gilibrator flow meter (Gilian Gilibrator-2, stated accuracy ±1%). The total uncertainty in the dilution factor is defined by the accuracy of the measurement of the dilution flows as well as by the accuracy of the flow controllers used for flow regulation (± 2 %) and was calculated to be 2.5 %. The error in the calculated reactivity is lowest for the lowest dilution but if the $[NO_3]_t^{Amb}$ gets close to the detection limit this will also have a strong influence on the calculated reactivities making a higher dilution factor favourable. Dilution factors were chosen to keep the instrument operating in a region (10 pptv < NO_3 < 40 pptv) where both effects are minimized.

A minimum detectable change in NO_3 of 2.5 pptv leads to an uncertainty of ≈ 15 %, when NO_3 varies between ≈ 10 und 30 pptv (starting from 50 pptv in zero-air). The uncertainty increases dramatically when NO_3 levels are close to 50 pptv (i.e. very low reactivity) or less than 5 pptv (very high reactivity without dilution). This is illustrated in Figure S1 of the supplementary information. As mentioned in section 2.3.1 the uncertainty in the reaction time (10 %) also contributes to the overall uncertainty.

To assess the uncertainty associated with derivation of the NO_3-reactivity from numerical simulation, uncertainties associated with the input parameters have to be considered. As previously demonstrated (Groß et al., 2014) this is best assessed in a Monte-Carlo approach in which the key parameters are varied within a range reflecting their uncertainty limits. The parameters that most sensitively influence the derived value of NO_3 reactivity are the NO_2 mixing ratio and the rate coefficients for N_2O_5 formation ($k_3 = 1.2 \pm 0.1 \times 10^{-12}$ cm^3 molecule^{-1} s^{-1}) and decomposition ($k_4 = 4.4 \pm 0.4 \times 10^{-2}$ cm^3 molecule^{-1} s^{-1}). The rate coefficients listed are for 1 bar and room temperature as appropriate for the experimental conditions, the uncertainties quoted (≈ 10 %) are based on assessment of kinetic data (Burkholder et al., 2016). The Monte Carlo simulations were initiated with a NO_3 mixing ratio (in zero-air) of 50 pptv, decreasing to 20 pptv upon reaction with air. In total, 6 sets of ≈ 1200 simulations were carried with variation of the initial NO_2 mixing ratio between 1 and 5 ppbv and the associated error in NO_2 mixing ratio was taken as 8 %. For any given simulation, the output value of the NO_3 reactivity (k_{RTG}) was stored. The 2σ uncertainty was derived from the Gaussian fits to histograms of k_{RTG} (insets at NO_2 = 1.0, 3.0 and 5.0 ppbv) and is plotted (as a percent of k_{RTG}) versus k_{RTG} / NO_2. The latter may be considered a measure of whether NO_3 reacts predominantly with NO_2 to form N_2O_5 (k_3) or with reactive trace gases. Fig. 11 shows that the uncertainty associated with the simulations is very sensitive to ambient NO_2 levels, varying between > 100 % (at 5 ppbv NO_2 and a reactivity of 0.017 s^{-1}) to 3.1 % (at 1 ppbv NO_2 and a reactivity of 0.092 s^{-1}) of the extracted k_{RTG}. Clearly, the extraction of k_{RTG} is most accurate in conditions of low NO_x and when NO_3 lifetimes are short (e.g. forested regions far from anthropogenic activity).

Another potential bias in the measurement is the temperature dependence of the rate constant of the reactions of trace gases with NO_3. Measurements were normally conducted at 20 °C in the flow-tube whilst outside temperature can differ from this. However, (unlike OH) the NO_3 reactions which dominate its reactivity involve addition to double bonds (e.g. of terpenes) and are only weakly temperature dependent. Therefore, to a good approximation, this error can generally be neglected. To illustrate this, we consider the reaction between NO_3 and the usually most abundant monoterpene, α-pinene. The rate

constant at the flow-tube temperature (20 °C) is 6.4×10^{-12} cm^3 $molecule^{-1}$ s^{-1} increasing to 7.0×10^{-12} cm^3 $molecule^{-1}$ s^{-1} at 5 °C and decreasing to 5.9×10^{-12} cm^3 $molecule^{-1}$ s^{-1} at 35 °C, which are changes of < 10 %. Note also that for many monoterpenes, the temperature dependence of the rate constant is not known, but expected to be weak (IUPAC, 2016).

Under circumstances where the reactivity is known to be driven by reaction with reactive trace gases for which NO_3 has large temperature dependence this error has to be taken into consideration.

We now examine the potential bias caused by use of NO_3 concentrations as large as 50 pptv, which may change the reactivity of the air either by removing a significant fraction of gas-phase reactants or via formation of peroxy radicals (RO_2), which may also react with NO_3. In a first scenario, we assume that the reactivity is caused by a single species, namely the generally dominant terpene, α-pinene and consider both low (k_{RTG} = 0.005 s^{-1}) and high reactivity regimes (k_{RTG} = 0.1 s^{-1}). A value of k_{RTG} = 0.005 s^{-1} would result if 34 pptv of α-pinene were available for reaction. In a first approximation, assuming first-order kinetics, we calculate that 2.5 pptv of the initially available 50 pptv of NO_3 are lost in the 10.5 s reaction time, and consequently a change in α-pinene of 2.5 pptv would also occur. This is only 7 % of the initial concentration, indicating an upper limit to a negative bias of 7 %. This is an upper limit as the assumption of first order kinetics is not entirely appropriate. As NO_3 reacts with α-pinene in air to form a nitroxy peroxy radical (RO_2) we also consider a positive bias due to reaction of NO_3 with this RO_2. To do this we assume a rate constant of 1.2×10^{-12} cm^3 $molecule^{-1}$ s^{-1} for the reaction as observed for $NO_3 + CH_3O_2$ (Atkinson et al., 2006) and assume that this rate constant is independent of the nature of the organic fragment (R) as is the case for reactions of RO_2 with NO. The 2.5 pptv RO_2 thus generated results in an incremental NO_3 reactivity of 7×10^{-5} s^{-1}, a positive bias of 1.5 %. Again, this is an upper limit, as the calculation assumes that this concentration of RO_2 is constant and available for the whole 10.5 s of reaction time. For higher reactivity (0.1 s^{-1}) a similar calculation shows that the 670 pptv required would reduce the NO_3 concentration to 17.5 pptv, itself being diminished to ~640 pptv, a change of just 5 %. The 32.5 pptv RO_2 generated would result in a loss rate constant for NO_3 of ~9×10^{-4} s^{-1}, a positive bias of ~ 1%. In conclusion, for reactive systems in which a large concentration of reactive trace gases with moderate reactivity towards NO_3 are encountered, we expect no significant bias. The only scenario, in which a large bias can ensue, is when a low reactivity is caused by a very low concentration of an extremely reactive traces gas. Taking the example of 1 pptv of a highly reactive terpenoid ($k = 2 \times 10^{-10}$ cm^3 $molecule^{-1}$ s^{-1}) it is easy to show that it would be reduced to just a few percent of its initial concentration when mixed with 50 pptv of NO_3 for 10.5 s. In this case a large negative bias would result. In the real atmosphere, this situation is however unlikely to occur as such reactive species are usually substantially reduced in concentration compared to the generally dominant biogenics such as α-pinene.

The overall uncertainty thus derives from a combination of measurement errors (cavity instability, drift in NO_3 source etc.) and the need to correct for NO_3 reactions with NO_2. Under ideal conditions (e.g. as described above for laboratory operation) the former can be reduced to ≈ 16 %. For a scenario in which biogenic VOCs dominate NO_3 reactivity in a low NO_x (< 1 ppbv) environment an additional uncertainty of ≈ 6-10 % from the numerical simulations results in a total uncertainty of

≈ 17-20 %. In a high NO_x environment, the total uncertainty will be dominated by that associated with the simulations. For example, at 5 ppbv NO_2 and a reactivity of 0.03 s^{-1} the total error would be close to 45-50 %.

6 Deployment in the NOTOMO campaign, 2015

The NO_3 reactivity set-up described above was deployed for the first time in the field during the NOTOMO campaign (NOcturnal chemistry at the Taunus Observatorium: insights into Mechanisms of Oxidation) in the Taunus mountains (S.W. Germany) in 2016. The site, previously described in detail (Crowley et al., 2010; Sobanski et al., 2016b), is situated on top of the "Kleiner Feldberg" mountain (850 m above sea level) in a forested area with urban influence. The site is impacted by biogenic emissions from forested regions (mainly in the north/west) and by anthropogenic emissions from the local urban centres of Frankfurt, Mainz and Wiesbaden in the south-east to south-west.

6.1 Reactivity measurements during NOTOMO

The NO_3 reactivity instrument was located in a research container and sampled from a common, high-flow inlet together with other instruments. The high-flow inlet was driven by an industrial fan drawing 10 m^3 min^{-1} through a 15 cm diameter stainless steel pipe with its opening about 8 m above the ground. This flow was sub-sampled with a 4 m length of ¼-inch PFA tubing that extracted the required 3300 sccm air from the centre of the stainless steel pipe and directed it through a 1 µm PFA filter to the NO_3-reactivity instrument. Due to thermostat break-down during NOTOMO, the NO_3-reactivity measurements were performed with the flow-tube at container temperature, which was variable (14 - 31 °C).

Previous campaigns at the Taunus Observatory have revealed occasionally high night-time mixing ratios of NO_3 and N_2O_5 (Sobanski et al., 2016b). As sampling NO_3 and N_2O_5 from ambient air would bias the NO_3-reactivity measurements to low values, a 2 l glass flask heated to ≈ 40-50 °C was placed at night in the ambient air stream to decompose N_2O_5 to NO_3 and NO_2. Based on its thermal dissociation rate coefficient (0.75 s^{-1} at 50 °C), N_2O_5 completely decomposes within the ≈ 40 s residence time in this glass vessel, and the NO_3 formed is expected to be lost on the uncoated glass walls, thus preventing reformation of N_2O_5. Measurements with ≈ 200 pptv of N_2O_5 added directly to the heated vessel and measured by the ambient and heated channels of the two-cavity CRDS (see section 2.2) confirmed that neither NO_3 nor N_2O_5 survived. As the N_2O_5 mixing ratio was measured during NOTOMO it is in principal possible to correct the data for the additional NO_2 thus generated. However, on most nights N_2O_5 levels were too low for this to have a significant effect. Further experiments with isoprene and α-pinene indicated that there was no significant change in NO_3-reactivity when the glass vessel was used or not, indicating no significant losses of these VOCs in the glass flask. We cannot exclude that other, less volatile organic trace gases including e.g. acids or peroxides may be lost in the glass vessel, but these are not expected to contribute significantly to NO_3 losses as their rate coefficients for reaction with NO_3 are generally too low. A further potential bias related to the use of the glass trap is the thermal decomposition of PAN and related peroxy nitrates, which can acquire concentrations of up to a few ppb at this site (Sobanski et al., 2016c; Thieser et al., 2016). If PAN decomposes in the glass vessel NO_2 will form,

thus contributing to the measured reactivity. Simulations indicate that during the 40 s residence time in the heated flask (at 50 °C) only a small fraction (≈ 2.6 %) of the PAN decomposes to form NO_2. For future experiments in environments of high NO_x with N_2O_5 and NO_3 present, the system will be operated at a lower temperature (e.g. 35 °C, τ_{PAN} = ~500 s, τ_{N2O5} = ~6 s) to make sure all of the N_2O_5/NO_3 is removed but PAN is preserved. We note that when measuring NO_3-reactivity in regions with large biogenic emissions, the use of the glass vessel to remove NO_3 and N_2O_5 is generally not necessary as high levels of biogenic VOCs and the low levels of NO_x often found in forested / rural environments remote from anthropogenic influence will result in very low levels of NO_3 or N_2O_5.

During NOTOMO, ambient levels of NO_2, NO_3, N_2O_5 and organic nitrates were measured with the CRDS instruments previously described by Sobanski et al. (Sobanski et al., 2016a; Thieser et al., 2016). The uncertainty in the measurements was 8 % for NO_2, 20 % for NO_3 whereas the uncertainty for PAN was highly variable for each data point (Sobanski et al., 2016c). The O_3 mixing ratios were measured using a dual beam ozone monitor (2B-Technology Model 202) with an uncertainty of 2 %. [NO] was not directly measured but its daytime concentration was calculated assuming photo-stationary-state via expression (12):

$$[NO]_{calc} = J(NO_2)\,[NO_2] / k_{(NO+O3)}[O_3] \quad (12)$$

where $J(NO_2)$ is the photolysis frequency of NO_2 and $k_{(NO+O3)}$ is the rate constant for reaction of NO with O_3. This expression ignores the oxidation of NO to NO_2 via e.g. reactions of peroxy radicals and thus overestimates NO. $J(NO_2)$ was measured using a spectral radiometer located close to the inlet (MetCon).

In this manuscript we focus on a three-day period, during which NO_3-reactivity was measured (Fig. 12a). The NO_3 reactivity, k_{RTG}, varied from 0.005 to 0.1 s^{-1} during night-time but reached values as high as 1.4 s^{-1} during daytime. The total uncertainty of the measurement is depicted by the amber, shaded area. The red line indicates that, as expected, daytime losses are dominated by reaction with NO (up to 1.3 s^{-1}). Night-time values of k_{RTG} were between 0.005 and 0.1 s^{-1}. Assuming that NO levels are close to zero as measured previously at this site during night-time (Crowley et al., 2010), k_{RTG} is then expected to be dominated by VOCs.

In Fig. 12b, we compare values of k_{RTG} obtained by rigorous data correction (black curve), to those calculated directly from expression (11) (blue curve). The simple analytical expression (blue line) results in an underestimation of the reactivity, especially during night, when the overall reactivity is low, and in periods of high $[NO_2]$. Owing to lack of temperature stabilization of the darkened reactor (at this time not yet incorporated) and break-down of the flow-tube thermostat during the campaign, temperature fluctuations in the container resulted in MDC_{NO3} = 5.6 pptv and hence an average, measureable reactivity of ≈ 0.01 s^{-1} during the campaign. As described in section 5 the minimum detectable change in NO_3 was combined with the uncertainty associated with the dilution factor, reaction time, $[NO_2]$, [PAN] and rate constants used to calculate the overall uncertainty for the reactivity at every data point. The overall uncertainty for the measurement period illustrated in Fig. 12 was ≈ 25 %.

In Fig. 13a/b we compare the measured night-time NO_3-reactivity with that obtained from the stationary-state analysis using expression (1). For the two nights in the period analysed, NO_3 mixing ratios were between 5 and 37 pptv ($[NO_3]$>> 5 pptv)

and the calculated stationary-state loss rate coefficients varied between 0.03-0.003 s^{-1} compared to the measured reactivity which was between 0.05-0.006 s^{-1} with a short time period in which k_{RTG} fell below the detection limit of the instrument. Within the total uncertainty, the measured and stationary-state reactivities are in reasonable agreement for most of the night from the 17th to the 18th. From the night 18th to the 19th the stationary-state reactivity is much lower (up to a factor of eight) than that measured. This difference and also the higher variability can be attributed to rapid variations in concentrations of VOCs at the inlet (due e.g. to emissions from nearby trees) that are not considered in the stationary-state approach; i.e. very local emissions of reactive gases will result in breakdown of the stationary-state assumption leading to the underestimation of the reactivity of the local mixture of VOCs and NO_x. As the direct measurement of the NO_3 reactivity with this device sums over all VOCs present in the air mass sampled, it should give the same result as summing each VOC concentration multiplied by the individual rate coefficients for reaction with NO_3, i.e NO_3 reactivity = $\sigma\ [VOC]_i k_i$. As demonstrated previously for this mountain site (Sobanski et al., 2016b), summed losses based on measurement of VOCs can significantly exceed the reactivity based on a stationary-state analysis especially under some meteorological situations in which a low-lying residual layer (with high NO_3 concentrations) influences the measurement.

7 Conclusion and outlook

We present the first instrument for measurement of NO_3 reactivity in ambient air. The flow-tube based instrument, utilizes the depletion of synthetically generated NO_3 when mixed with ambient air and has a dynamic range of 0.005 s^{-1} to 45s^{-1}. Following intensive laboratory characterization to determine the effective reaction time, the wall loss constant of NO_3 and the effect of NO_3 formation and reformation in the flow-tube, it was successfully tested against an isoprene standard. The overall uncertainty depends on the relative rate of reaction of NO_3 with NO_2 or with other traces gases (e.g. VOCs or NO) that do not generate N_2O_5 and which, under ideal conditions, is close to 15 %. The instrument is thus best suited for measurement of NO_3 reactivity in regions with high biogenic activity and relatively low direct anthropogenic emissions of NO_x, i.e. regions where the measurement of NO_3 concentrations is difficult owing to low production rates and a high loss term.

First deployment of the instrument was during the NOTOMO observational experiment in summer 2015 at a forested, mountain site with urban influence. The measured NO_3 reactivity ranged from 0.006 to 0.1 to s^{-1} at night-time and reached values as high as 1.4 s^{-1} during daytime. As expected, daytime reactivity was dominated by reaction with NO while night-time reactivity involved other (presumably organic) trace gases. A comparison with stationary-state calculations of the NO_3 reactivity revealed poor agreement on occassions, presumably related to very local emissions causing a breakdown of the stationary-state assumption.

Improvements to the dynamic range of the instrument require further stabilization of the NO_3 source and cavity-optics to reduce the minimal detectable change in NO_3 (presently MDC_{NO3} = 2.5 pptv). This could also be achieved by the use of larger volume flow-tubes. Reduction in the initial NO_3 concentration used would also reduce any potential bias caused by

595 depletion of reactants or secondary chemistry. Future deployment with simultaneous measurements of NO_3, NO_2, O_3 and
596 VOCs will be conducted to compare direct measurements of NO_3 reactvity with those obtained from the stationary-state
597 approach and also those calculated from summing losses to individual VOCs.

598 **Acknowledgements**

599 We would like to thank Heinz Bingemer and the staff and department of the Johann Wolfgang Goethe–University, Frankfurt
600 am Main for logistical support and access to the Taunus Observatory during NOTOMO. We also would like to thank Eva
601 Pfannerstil for providing the isoprene standard. We thank DuPont for the sample of FEP used to coat the walls of the flow
602 tube and darkened reactor. This work was carried out in partial fulfilment of the PhD (Johannes Gutenberg University,
603 Mainz, Germany) of Jonathan Liebmann.
604

References

Atkinson, R.: Atmospheric chemistry of VOCs and NOx, Atmos. Env., 34, 2063-2101, 2000.

Atkinson, R., and Arey, J.: Gas-phase tropospheric chemistry of biogenic volatile organic compounds: a review, Atmos. Env., 37, S197-S219, 2003a.

Atkinson, R., and Arey, J.: Atmospheric degradation of volatile organic compounds, Chem. Rev., 103, 4605-4638, 10.1021/cr0206420, 2003b.

Atkinson, R., Baulch, D. L., Cox, R. A., Crowley, J. N., Hampson, R. F., Hynes, R. G., Jenkin, M. E., Rossi, M. J., and Troe, J.: Evaluated kinetic and photochemical data for atmospheric chemistry: Volume I - gas phase reactions of O*x*, HO*x*, NO*x* and SO*x* species, Atmos. Chem. Phys., 4, 1461-1738, 2004.

Atkinson, R., Baulch, D. L., Cox, R. A., Crowley, J. N., Hampson, R. F., Hynes, R. G., Jenkin, M. E., Rossi, M. J., and Troe, J.: Evaluated kinetic and photochemical data for atmospheric chemistry: Volume II - reactions of organic species, Atmos. Chem. Phys., 3625-4055, 2006.

Berden, G., Peeters, R., and Meijer, G.: Cavity ring-down spectroscopy: Experimental schemes and applications, International Reviews in Physical Chemistry, 19, 565-607, 2000.

Brown, S. S., Stark, H., and Ravishankara, A. R.: Cavity ring-down spectroscopy for atmospheric trace gas detection: application to the nitrate radical (NO3), Applied Physics B-Lasers and Optics, 75, 173-182, 2002.

Brown, S. S., Stark, H., and Ravishankara, A. R.: Applicability of the steady state approximation to the interpretation of atmospheric observations of NO_3 and N_2O_5, J. Geophys. Res. -Atmos., 108, Art. 4539, 10.1029/2003JD003407, 2003.

Brown, S. S., Dube, W. P., Osthoff, H. D., Stutz, J., Ryerson, T. B., Wollny, A. G., Brock, C. A., Warneke, C., De Gouw, J. A., Atlas, E., Neuman, J. A., Holloway, J. S., Lerner, B. M., Williams, E. J., Kuster, W. C., Goldan, P. D., Angevine, W. M., Trainer, M., Fehsenfeld, F. C., and Ravishankara, A. R.: Vertical profiles in NO3 and N2O5 measured from an aircraft: Results from the NOAA P-3 and surface platforms during the New England Air Quality Study 2004, J. Geophys. Res. -Atmos., 112, D22304, doi: 10.1029/2007jd008893, 2007a.

Brown, S. S., Dube, W. P., Osthoff, H. D., Wolfe, D. E., Angevine, W. M., and Ravishankara, A. R.: High resolution vertical distributions of NO_3 and N_2O_5 through the nocturnal boundary layer, Atmos. Chem. Phys., 7, 139-149, 2007b.

Brown, S. S., Dube, W. P., Fuchs, H., Ryerson, T. B., Wollny, A. G., Brock, C. A., Bahreini, R., Middlebrook, A. M., Neuman, J. A., Atlas, E., Roberts, J. M., Osthoff, H. D., Trainer, M., Fehsenfeld, F. C., and Ravishankara, A. R.: Reactive uptake coefficients for N_2O_5 determined from aircraft measurements during the Second Texas Air Quality Study: Comparison to current model parameterizations, J. Geophys. Res. -Atmos., 114, art. D00F10, 10.1029/2008JD011679, 2009.

Brown, S. S., and Stutz, J.: Nighttime radical observations and chemistry, Chem. Soc. Rev., 41, 6405–6447, 2012.

Burkholder, J. B., Sander, S. P., Abbatt, J., Barker, J. R., Huie, R. E., Kolb, C. E., Kurylo, M. J., Orkin, V. L., Wilmouth, D. M., and Wine, P. H.: Chemical Kinetics and Photochemical Data for Use in Atmospheric Studies, Evaluation No. 18," JPL Publication 15-10, Jet Propulsion Laboratory, Pasadena, http://jpldataeval.jpl.nasa.gov., 2016.

Crowley, J. N., Schuster, G., Pouvesle, N., Parchatka, U., Fischer, H., Bonn, B., Bingemer, H., and Lelieveld, J.: Nocturnal nitrogen oxides at a rural mountain site in south-western Germany, Atmos. Chem. Phys., 10, 2795-2812, 2010.

Crowley, J. N., Thieser, J., Tang, M. J., Schuster, G., Bozem, H., Hasaynali Beygi, Z., Fischer, H., Diesch, J.-M., Drewnick, F., Borrmann, S., Song, W., Yassaa, N., Williams, J., Pöhler, D., Platt, U., and Lelieveld, J.: Variable lifetimes and loss mechanisms for NO_3 and N_2O_5 during the DOMINO campaign: Contrast between marine, urban and continental air, Atmos. Chem. Phys., 11, 10863-10870, 2011.

Crutzen, P.: A discussion of the chemistry of some minor constituents in the stratosphere and troposphere, Pure and Applied Geophysics, 106-108, 1385-1399, 1973.

Curtis, A. R., and Sweetenham, W. P.: Facsimile, AERE, Report R-12805, in, 1987.

Dentener, F. J., and Crutzen, P. J.: Reaction of N_2O_5 on tropospheric aerosols - Impact on the global distributions of NO_x, O_3, and OH, J. Geophys. Res. -Atmos., 98, 7149-7163, 1993.

Donahue, N. M., Clarke, J. S., Demerjian, K. L., and Anderson, J. G.: Free-radical kinetics at high pressure: A mathematical analysis of the flow reactor, J. Phys. Chem., 100, 5821-5838, 1996.

Fry, J. L., Draper, D. C., Barsanti, K. C., Smith, J. N., Ortega, J., Winkle, P. M., Lawler, M. J., Brown, S. S., Edwards, P. M., Cohen, R. C., and Lee, L.: Secondary Organic Aerosol Formation and Organic Nitrate Yield from NO_3 Oxidation of Biogenic Hydrocarbons, Env. Sci. Tech., 48, 11944-11953, 10.1021/es502204x, 2014.

Fuchs, H., Dube, W. P., Cicioira, S. J., and Brown, S. S.: Determination of inlet transmission and conversion efficiencies for in situ measurements of the nocturnal nitrogen oxides, NO3, N2O5 and NO2, via pulsed cavity ring-down spectroscopy, Anal. Chem., 80, 6010-6017, 2008.

Geyer, A., and Platt, U.: Temperature dependence of the NO3 loss frequency: A new indicator for the contribution of NO3 to the oxidation of monoterpenes and NOx removal in the atmosphere, J. Geophys. Res. -Atmos., 107, 4431, doi:10.1029/2001JD001215, 10.1029/2001JD001215, 2002.

Groß, C. B. M., Dillon, T. J., Schuster, G., Lelieveld, J., and Crowley, J. N.: Direct kinetic study of OH and O_3 formation in the reaction of $CH_3C(O)O_2$ with HO_2, The Journal of Physical Chemistry A, 118, 974-985, doi:10.1021/jp412380z, 2014.

Guenther, A. B., Jiang, X., Heald, C. L., Sakulyanontvittaya, T., Duhl, T., Emmons, L. K., and Wang, X.: The Model of Emissions of Gases and Aerosols from Nature version 2.1 (MEGAN2.1): an extended and updated framework for modeling biogenic emissions, Geoscientific Model Development, 5, 1471-1492, 10.5194/gmd-5-1471-2012, 2012.

Heintz, F., Platt, U., Flentje, H., and Dubois, R.: Long-term observation of nitrate radicals at the tor station, Kap Arkona (Rugen), J. Geophys. Res. -Atmos., 101, 22891-22910, 1996.

Howard, C. J.: Kinetic measurements using flow tubes, J. Phys. Chem., 83, 3-9, 1979.

Huang, Y., Shen, H. Z., Chen, Y. L., Zhong, Q. R., Chen, H., Wang, R., Shen, G. F., Liu, J. F., Li, B. G., and Tao, S.: Global organic carbon emissions from primary sources from 1960 to 2009, Atmos. Env., 122, 505-512, 10.1016/j.atmosenv.2015.10.017, 2015.

Huang, Y., Coggon, M. M., Zhao, R., Lignell, H., Bauer, M. U., Flagan, R. C., and Seinfeld, J. H.: The Caltech Photooxidation Flow Tube Reactor - I: Design and Fluid Dynamics, Atmos. Meas. Tech. Discuss., 2016, 1-36, 10.5194/amt-2016-282, 2016.

IUPAC: Task Group on Atmospheric Chemical Kinetic Data Evaluation, (Ammann, M., Cox, R.A., Crowley, J.N., Herrmann, H., Jenkin, M.E., McNeill, V.F., Mellouki, A., Rossi, M. J., Troe, J. and Wallington, T. J.) http://iupac.pole-ether.fr/index.html., http://iupac.pole-ether.fr/index.html., 2016.

Kovacs, T. A., and Brune, W. H.: Total OH loss rate measurement, J. Atmos. Chem., 39, 105-122, 10.1023/a:1010614113786, 2001.

Lelieveld, J., Butler, T. M., Crowley, J. N., Dillon, T. J., Fischer, H., Ganzeveld, L., Harder, H., Lawrence, M. G., Martinez, M., Taraborrelli, D., and Williams, J.: Atmospheric oxidation capacity sustained by a tropical forest, Nature, 452, 737-740, 2008.

Lelieveld, J., Gromov, S., Pozzer, A., and Taraborrelli, D.: Global tropospheric hydroxyl distribution, budget and reactivity, Atmos. Chem. Phys. Discuss., 2016, 1-25, 10.5194/acp-2016-160, 2016.

Mielke, L. H., Furgeson, A., and Osthoff, H. D.: Observation of $ClNO_2$ in a mid-continental urban environment, Env. Sci. Tech., 45, 8889-8896, doi:10.1021/es201955u, 2011.

Mogensen, D., Gierens, R., Crowley, J. N., Keronen, P., Smolander, S., Sogachev, A., Nölscher, A. C., Zhou, L., Kulmala, M., Tang, M. J., Williams, J., and Boy, M.: Simulations of atmospheric OH, O_3 and NO_3 reactivities within and above the boreal forest, Atmos. Chem. Phys., 15, 3909-3932, 10.5194/acp-15-3909-2015, 2015.

Ng, N. L., Brown, S. S., Archibald, A. T., Atlas, E., Cohen, R. C., Crowley, J. N., Day, D. A., Donahue, N. M., Fry, J. L., Fuchs, H., Griffin, R. J., Guzman, M. I., Hermann, H., Hodzic, A., Iinuma, Y., Jimenez, J. L., Kiendler-Scharr, A., Lee, B. H., Luecken, D. J., Mao, J., McLaren, R., Mutzel, A., Osthoff, H. D., Ouyang, B., Picquet-Varrault, B., Platt, U., Pye, H. O. T., Rudich, Y., Schwantes, R. H., Shiraiwa, M., Stutz, J., Thornton, J. A., Tilgner, A., Williams, B. J., and Zaveri, R. A.: Nitrate radicals and biogenic volatile organic compounds: oxidation, mechanisms and organic aerosol, Atmos. Chem. Phys. Discuss., 2016, 1-111, 10.5194/acp-2016-734, 2016.

Orphal, J., Fellows, C. E., and Flaud, P. M.: The visible absorption spectrum of NO3 measured by high-resolution Fourier transform spectroscopy, J. Geophys. Res. -Atmos., 108, Art. Nr. 4077, doi:10.1029/2002JD002489, 2003.

Osthoff, H. D., Pilling, M. J., Ravishankara, A. R., and Brown, S. S.: Temperature dependence of the NO_3 absorption cross-section above 298 K and determination of the equilibrium constant for $NO_3 + NO_2 <-> N_2O_5$ at atmospherically relevant conditions, Phys. Chem. Chem. Phys., 9, 5785-5793, 2007.

Osthoff, H. D., Roberts, J. M., Ravishankara, A. R., Williams, E. J., Lerner, B. M., Sommariva, R., Bates, T. S., Coffman, D., Quinn, P. K., Dibb, J. E., Stark, H., Burkholder, J. B., Talukdar, R. K., Meagher, J., Fehsenfeld, F. C., and Brown, S. S.: High levels of nitryl chloride in the polluted subtropical marine boundary layer, Nature Geoscience, 1, 324-328, 2008.

Phillips, G. J., Tang, M. J., Thieser, J., Brickwedde, B., Schuster, G., Bohn, B., Lelieveld, J., and Crowley, J. N.: Significant concentrations of nitryl chloride observed in rural continental Europe associated with the influence of sea salt chloride and anthropogenic emissions, Geophys. Res. Lett., 39, L10811, doi:10.1029/2012GL051912, 2012.

Riedel, T. P., Bertram, T. H., Crisp, T. A., Williams, E. J., Lerner, B. M., Vlasenko, A., Li, S. M., Gilman, J., de Gouw, J., Bon, D. M., Wagner, N. L., Brown, S. S., and Thornton, J. A.: Nitryl Chloride and Molecular Chlorine in the Coastal Marine Boundary Layer, Env. Sci. Tech., 46, 10463-10470, 10.1021/es204632r, 2012.

Rinne, J., Markkanen, T., Ruuskanen, T. M., Petaja, T., Keronen, P., Tang, M. J., Crowley, J. N., Rannik, U., and Vesala, T.: Effect of chemical degradation on fluxes of reactive compounds –a study with a stochastic Lagrangian transport model, Atmos. Chem. Phys., 12, 4843-4854, 2012.

Schuster, G., Labazan, I., and Crowley, J. N.: A cavity ring down / cavity enhanced absorption device for measurement of ambient NO_3 and N_2O_5, Atmos. Meas. Tech., 2, 1-13, 2009.

Seeley, J. V., Jayne, J. T., and Molina, M. J.: High-Pressure Fast-Flow Technique for Gas-Phase Kinetics Studies, Int. J. Chem. Kinet., 25, 571-594, 1993.

Sinha, V., Williams, J., Crowley, J. N., and Lelieveld, J.: The comparative reactivity method - a new tool to measure total OH reactivity in ambient air, Atmos. Chem. Phys., 8, 2213-2227, 2008.

Sobanski, N., Schuladen, J., Schuster, G., Lelieveld, J., and Crowley, J. N.: A five-channel cavity ring-down spectrometer for the detection of NO2, NO3, N2O5, total peroxy nitrates and total alkyl nitrates, Atmos. Meas. Tech., 9, 5103-5118, 10.5194/amt-9-5103-2016, 2016a.

Sobanski, N., Tang, M. J., Thieser, J., Schuster, G., Pöhler, D., Fischer, H., Song, W., Sauvage, C., Williams, J., Fachinger, J., Berkes, F., Hoor, P., Platt, U., Lelieveld, J., and Crowley, J. N.: Chemical and meteorological influences on the lifetime of NO_3 at a semi-rural mountain site during PARADE, Atmos. Chem. Phys., 16, 4867-4883, 10.5194/acp-16-4867-2016, 2016b.

Sobanski, N., Thieser, J., Schuladen, J., Sauvage, C., Song, W., Williams, J., lelieveld, J., and Crowley, J. N.: Day- and Night-time Formation of Organic Nitrates at a Forested Mountain-site in South West Germany, Atmos. Chem. Phys. Discuss., submitted, 2016c.

Thieser, J., Schuster, G., Phillips, G. J., Reiffs, A., Parchatka, U., Pöhler, D., Lelieveld, J., and Crowley, J. N.: A two-channel, thermal dissociation cavity-ringdown spectrometer for the detection of ambient NO_2, RO_2NO_2 and $RONO_2$, Atmos. Meas. Tech., 9, 553-576, 2016.

Thornton, J. A., Kercher, J. P., Riedel, T. P., Wagner, N. L., Cozic, J., Holloway, J. S., Dube, W. P., Wolfe, G. M., Quinn, P. K., Middlebrook, A. M., Alexander, B., and Brown, S. S.: A large atomic chlorine source inferred from mid-continental reactive nitrogen chemistry, Nature, 464, 271-274, 10.1038/nature08905, 2010.

Wagner, N. L., Dube, W. P., Washenfelder, R. A., Young, C. J., Pollack, I. B., Ryerson, T. B., and Brown, S. S.: Diode laser-based cavity ring-down instrument for NO_3, N_2O_5, NO, NO_2 and O_3 from aircraft, Atmos. Meas. Tech., 4, 1227-1240, 10.5194/amt-4-1227-2011, 2011.

Wayne, R. P., Barnes, I., Biggs, P., Burrows, J. P., Canosa-Mas, C. E., Hjorth, J., Le Bras, G., Moortgat, G. K., Perner, D., Poulet, G., Restelli, G., and Sidebottom, H.: The nitrate radical: Physics, chemistry, and the atmosphere, Atmos. Env. A, 25A, 1-206, 1991.

731 **Table 1:** Facsimile[1] Simulations

732

$NO_2+O_3 \rightarrow NO_3 + O_2$	$k_1 = 3.52 \times 10^{-17}$ cm^3 molecule^{-1} s^{-1}	k_1
$NO_3 + NO \rightarrow 2\ NO_2$	$k_2 = 2.60 \times 10^{-11}$ cm^3 molecule^{-1} s^{-1}	k_2
$NO_3 + NO_2 + M \rightarrow N_2O_5 + M$	$k_3 = 1.24 \times 10^{-12}$ cm^3 molecule^{-1} s^{-1}	k_3
$N_2O_5 + M \rightarrow NO_2 + NO_3 + M$	$k_4 = 4.44 \times 10^{-2}$ cm^3 molecule^{-1} s^{-1}	k_4
$NO+O_3 \rightarrow NO_2 + O_2$	$k_5 = 1.89 \times 10^{-14}$ cm^3 molecule^{-1} s^{-1}	k_5
$NO_3 + wall \rightarrow NO_2$	$k_w = 4 \times 10^{-3}$ s^{-1}	k_w
k_{RTG}	variable / fitted	k_{RTG}

733 [1]For all simulations FACSIMILE-CHEKMAT (Release H010 DATE 28.04.87 Version 1) was used. The rate constants (k_i) listed were
734 taken from the IUPAC recommendations (Atkinson et al., 2004; IUPAC, 2016) at 298 K and 1 bar.

735

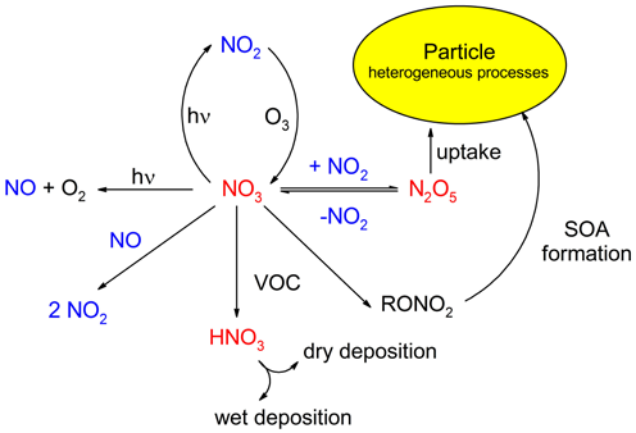

Figure 1: Gas-phase formation and loss of tropospheric NO_3.
SOA = secondary organic aerosol, $RONO_2$ are alkyl-nitrates.

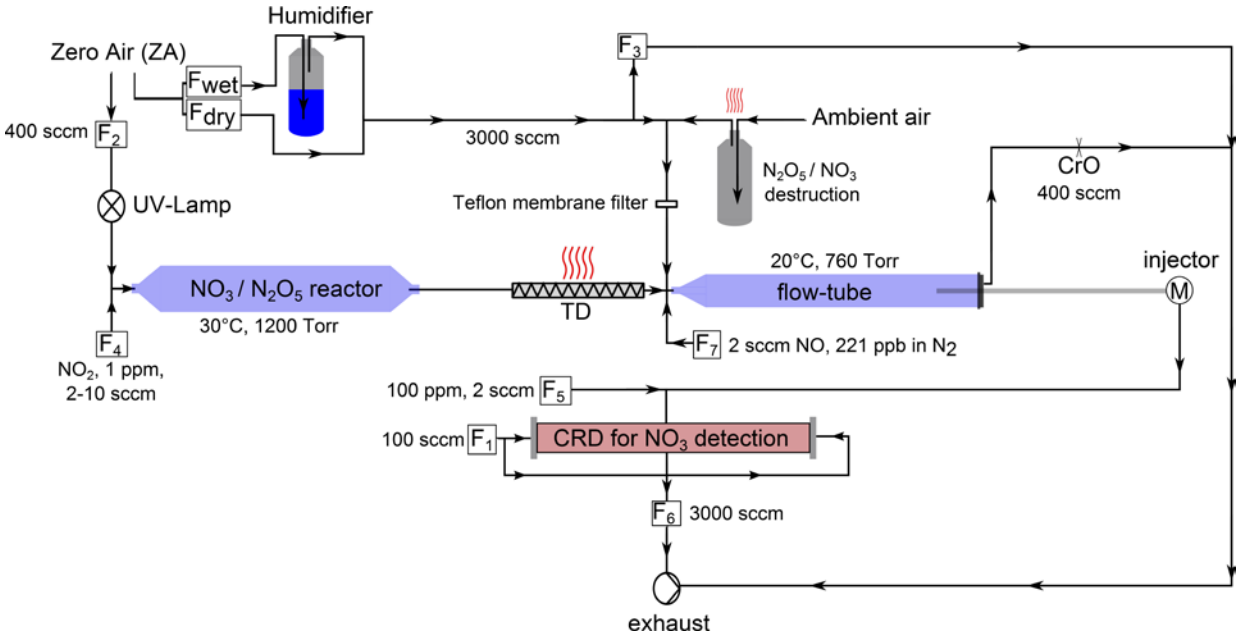

Figure 2: Schematic diagram of the NO_3-reactivity measurement. F_1-F_7 are mass flow-controllers: F_1 = mirror purge flow, F_2 = zero-air for O_3 generation, F_3 = dilution / inlet overflow (switching between zero-air and ambient), F_4 = NO_2 for NO_3 / N_2O_5 generation, F_5 = NO titration of NO_3, F_6 = cavity flow to pump, F_7 = NO flow for online reactivity calibration. CrO = critical orifice. TD = heated tubing for thermal decomposition of N_2O_5 to NO_3 at 140 °C.

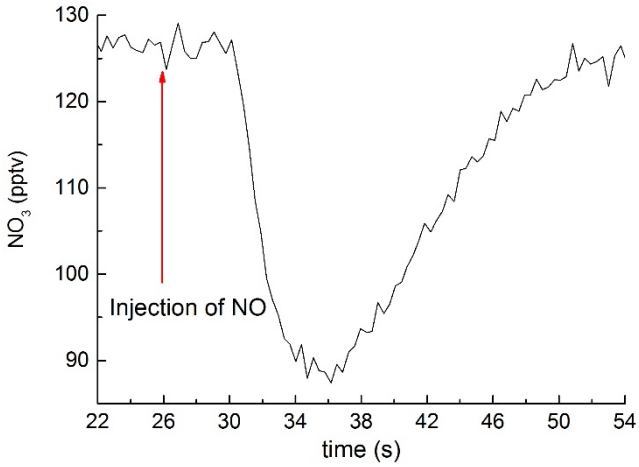

Figure 3: Derivation of effective reaction time by addition of a pulse (at t = 26 s) of NO using a syringe. The subsequent depletion in the NO_3 signal was analysed using expression 4.

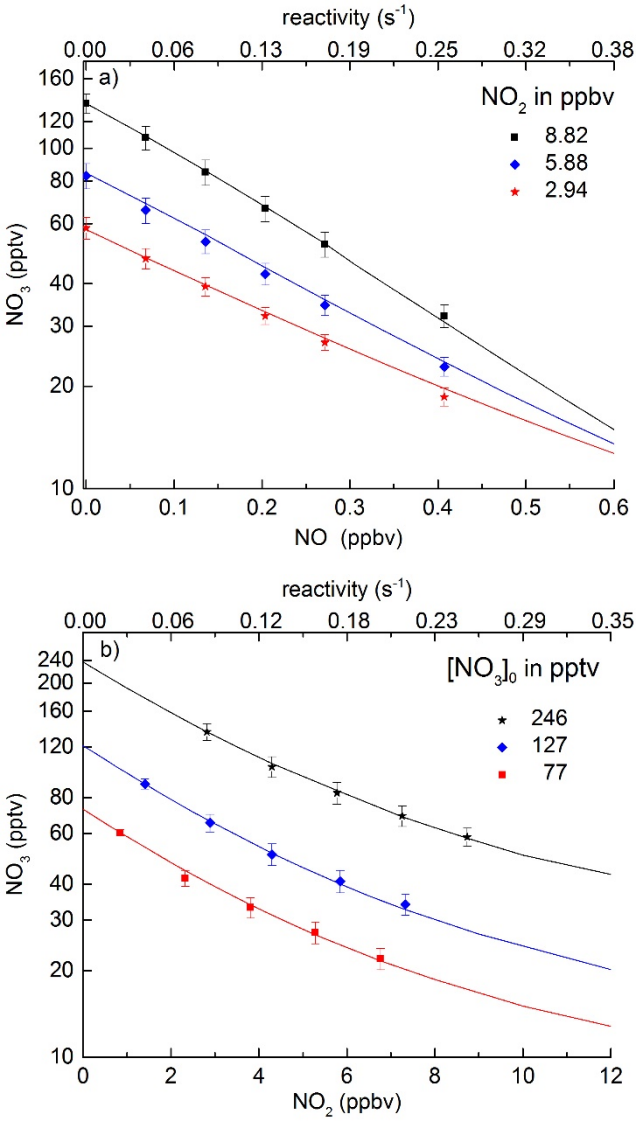

Figure 4: Characterisation of the flow-tube by numerical simulation of the NO_3 change following addition of NO and NO_2 at different mixing ratios. The symbols are measured NO_3 mixing ratios, the lines are the results of numerical simulations. The reactivity scales were calculated from k_2[NO] and k_3[NO_2] using the rate constants listed in Table 1.

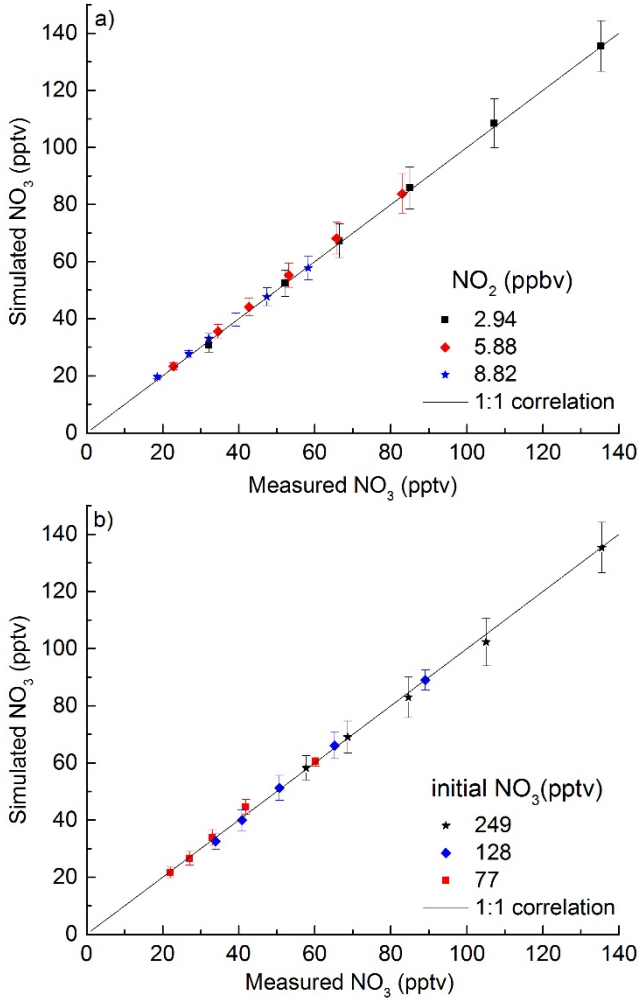

Figure 5: *Left:* Measured versus simulated NO_3 for different amounts of added NO (67, 134, 201, 268, 402 pptv) and at three different mixing ratios of NO_2. *Right*: Measured versus simulated NO_3 (initially 77, 128 or 249 pptv) at different amounts (1.5, 3, 4.5, 6 ppbv) of added [NO_2]. The solid lines represent 1:1 agreement.

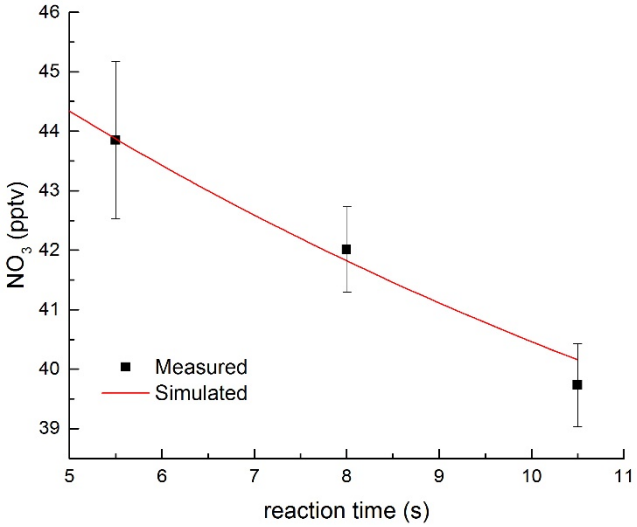

Figure 6: Determination of the NO_3 wall loss constant by variation of the reaction time (injector position). The simulation indicates a wall loss constant of $k_w = 0.004\ s^{-1}$.

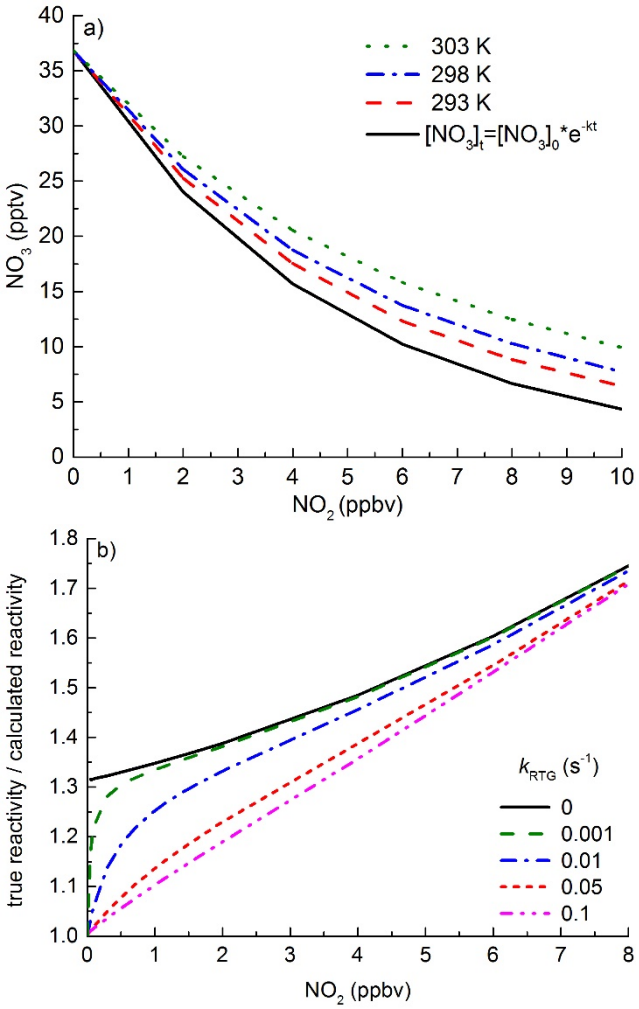

Figure 7: Influence of N_2O_5 formation and decomposition in the flow-tube. a) simulated (red, blue and green) mixing ratio of NO_3 versus added NO_2 at a reaction time of 10.5 s at various temperatures and thus thermal decomposition rates of N_2O_5. The simple exponential decay of NO_3 (expression 9) is given by the black line. b) Effect of NO_2 level on the ratio of true reactivity / reactivity calculated from expression (8) for different loss rate constants for NO_3 reacting with reactive traces gases.

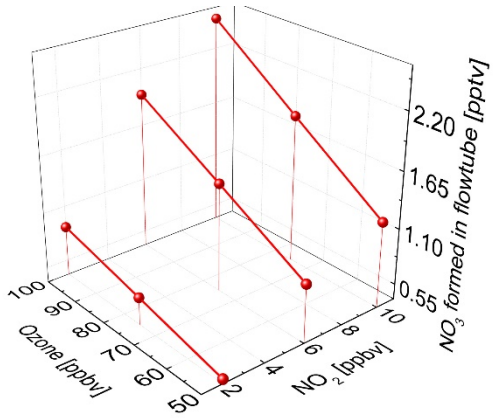

Figure 8: Simulated NO_3 production in the flow-tube at different O_3 and NO_2 mixing ratios at a fixed reaction time of 10.5 s.

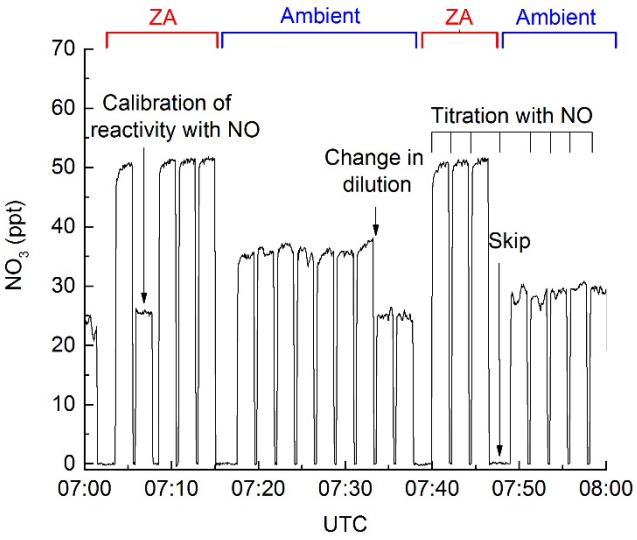

Figure 9: Raw data showing the change in NO_3 (10.5 s reaction time) between zero-air (ZA, periods marked with red brackets) and ambient air (Ambient, blue brackets). The Figure also shows periods of titration of NO_3 with NO (≈ 2 min intervals) a change in the dilution factor from 4 to 3 (at ≈ 07:33) and an in-situ reactivity calibration (at ≈ 07:07). The "skip" periods are those in which data are not analysed due to switching from ambient air to zero-air and vice versa.

901

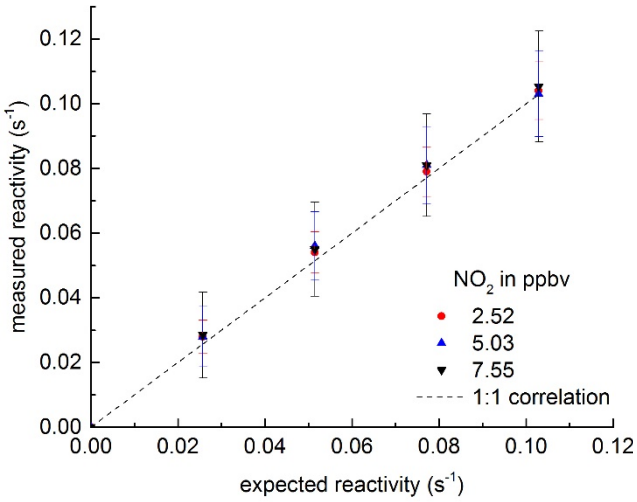

Figure 10: Verification of the experimental procedure by addition of isoprene at different NO_2 mixing ratios. The known reactivity was calculated from the isoprene mixing ratio (1.5 – 6 ppbv) and the rate coefficient for reaction of isoprene with NO_3. Experiments were performed in dry zero-air. The error bars in the simulation are due to uncertainties in [isoprene] and [NO_2] (both 5 %) and the reaction time (10 %).

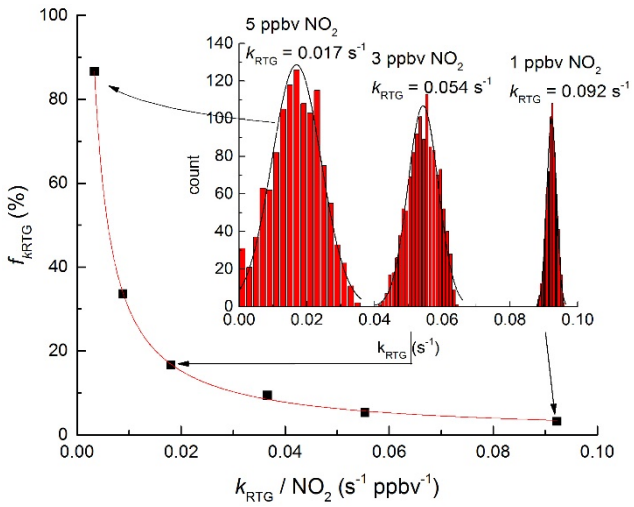

Figure 11: Uncertainty factor ($f\,k_{RTG}$) as a function of the ratio k_{RTG} / [NO_2] as derived from Monte-Carlo simulations. The relationship (black line) is described by $f\,(k_{RTG}) = 0.33 \times (k_{RTG} / [NO_2])^{-0.977}$. The results of three individual sets of 1200 simulations are shown as histograms.

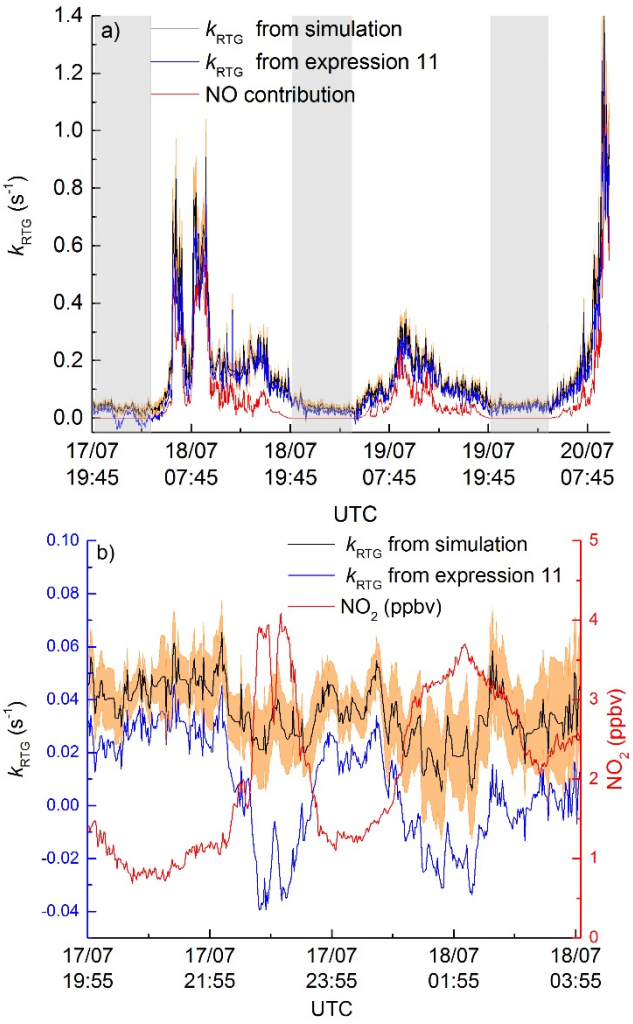

Figure 12: a) Measured values of k_{RTG} over a 3 day period. The overall uncertainty is represented by the amber, shaded area. The black lines are k_{RTG} obtained by full simulations, the blue lines are calculated using expression (11) (without correction for N_2O_5 formation and decomposition). The contribution of NO to the NO_3 reactivity is displayed as the red line. Yellow regions correspond to daytime, grey regions correspond to night-time b) Zoom in on a night-time period with low reactivity emphasizing the effect of NO_2-induced formation and decomposition of N_2O_5.

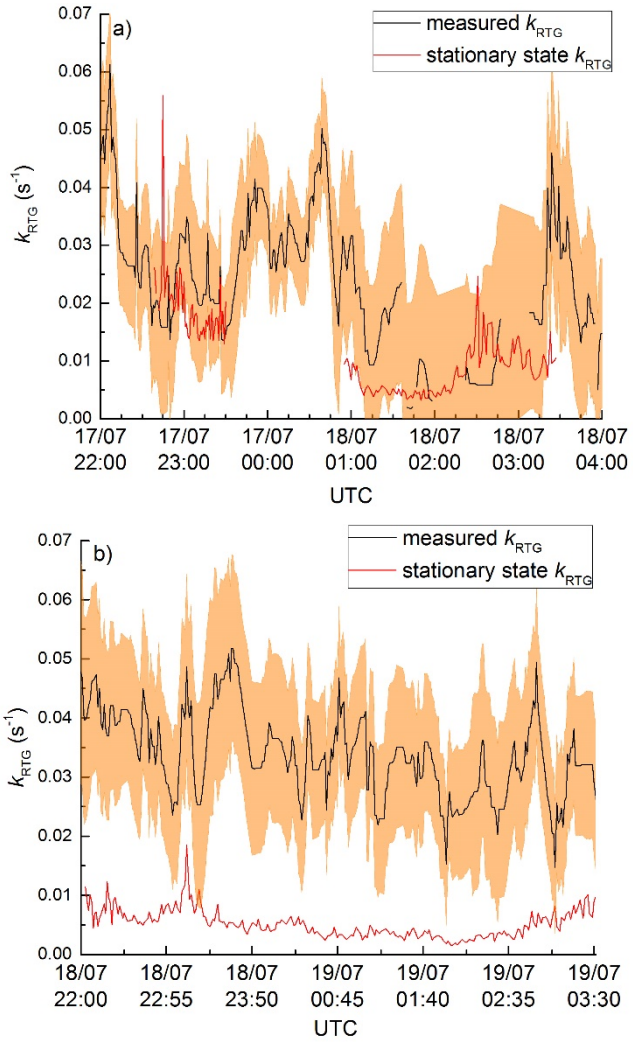

Figure 13: Comparison of stationary-state and measured NO_3 loss rates. Uncertainty in k_{RTG} (see text) are displayed as the amber shaded area.